Constraining plateau uplift in southern Africa by combining thermochronology, sediment flux, topography, and landscape evolution modeling

Jessica R. Stanley[1], Jean Braun[2], Guillaume Baby[3], François Guillocheau[4], Cecile Robin[5], Rebecca Flowers[6], Roderick Brown[7], Mark Wildman[7], and Romain Beucher[8]

[1]University of Idaho
[2]GeoForschungsZentrum Potsdam
[3]IPGP
[4]Geosciences Rennes - Universite Rennes 1
[5]University Rennes1
[6]University of Colorado Boulder
[7]University of Glasgow
[8]The Australian National University

November 26, 2022

Abstract

The uplift of the southern African Plateau is often attributed to mantle processes, but there are conflicting theories for the specific timing and drivers of topographic development. Evidence for most proposed plateau development histories is derived from continental erosion histories, marine stratigraphic architecture, or landscape morphology. Here we use a landscape evolution model to integrate these three types of data for southern Africa, including a large dataset of low temperature thermochronology, sediment flux rates to surrounding marine basins. We explore three main hypotheses for surface uplift: 1) southern Africa was already elevated at the time of Gondwana breakup, 2) uplift and continental tilting occurred in the mid-Cretaceous, or 3) uplift occurred in the mid to late Cenozoic. We test which of these three intervals of plateau development are plausible by using an inversion method to constrain the range in erosional and uplift model parameters that can best reproduce the observed data. Results indicate two families of uplift histories are most compatible with the data. Both have limited initial topography with some topographic uplift and continental tilting starting in the east at ~95 Ma. In one acceptable scenario, nearly all of the topography, ~1400 m, is created at this time with little Cenozoic uplift. In the other acceptable scenario, only ~500 m of uplift occurs in the mid-Cretaceous with another ~850 m of uplift in the mid-Cenozoic. The two model scenarios have different geodynamic implications, which in the future could be evaluated by direct comparison between geodynamic and landscape model predictions.

Constraining plateau uplift in southern Africa by combining thermochronology, sediment flux, topography, and landscape evolution modeling

Jessica R. Stanley[1], Jean Braun[2,3], Guillaume Baby[4], François Guillocheau[5], Cécile Robin[5], Rebecca M. Flowers[6], Roderick Brown[7], Mark Wildman[7], Romain Beucher[8]

[1] Department of Geological Sciences, University of Idaho, 875 Perimeter Dr MS3022, Moscow ID 83843, USA.

[2] Helmholtz Centre Potsdam, GFZ German Research Center for Geosciences, Telegrafenberg Building A27, 14473 Potsdam, Germany.

[3] Institut für Erd- und Umweltwissenschaften, Universität Potsdam, 14476 Potsdam, Germany.

[4] Université de Paris, Institut de Physique du Globe de Paris, CNRS, F-75005, Paris, France.

[5] Université de Rennes 1, CNRS, Géosciences Rennes - UMR 6118, 35000 Rennes, France.

[6] Department of Geological Sciences, University of Colorado Boulder, UCB399, Boulder CO 80309, USA.

[7] School of Geographical and Earth Sciences, University of Glasgow, Glasgow, Scotland.

[8] Research School of Earth Sciences, The Australian National University, Canberra ACT 2600, Australia.

Corresponding author: Jessica R. Stanley (jessicastanley@uidaho.edu)

Key Points:

- Hypotheses for southern African Plateau uplift are tested using large scale landscape model inversions
- Comparison of models to published thermochronology, sediment flux volumes, and topography highlight two suitable uplift histories
- Data cannot distinguish between these two models, which have different geodynamic implications, but do highlight areas for future work

Abstract

The uplift of the southern African Plateau is often attributed to mantle processes, but there are conflicting theories for the specific timing and drivers of topographic development. Evidence for most proposed plateau development histories is derived from continental erosion histories, marine stratigraphic architecture, or landscape morphology. Here we use a landscape evolution model to integrate these three types of data for southern Africa, including a large dataset of low temperature thermochronology, sediment flux rates to surrounding marine basins. We explore three main hypotheses for surface uplift: 1) southern Africa was already elevated at the time of Gondwana breakup, 2) uplift and continental tilting occurred in the mid-Cretaceous, or 3) uplift occurred in the mid to late Cenozoic. We test which of these three intervals of plateau development are plausible by using an inversion method to constrain the range in erosional and uplift model parameters that can best reproduce the observed data. Results indicate two families of uplift histories are most compatible with the data. Both have limited initial topography with some topographic uplift and continental tilting starting in the east at ~95 Ma. In one acceptable scenario, nearly all of the topography, ~1400 m, is created at this time with little Cenozoic uplift. In the other acceptable scenario, only ~500 m of uplift occurs in the mid-Cretaceous with another ~850 m of uplift in the mid-Cenozoic. The two model scenarios have different geodynamic implications, which in the future could be evaluated by direct comparison between geodynamic and landscape model predictions.

Plain Language Summary

How the southern African Plateau and its high elevations formed is disputed. The plateau is located far from tectonic plate boundaries, and many have suggested that processes below the crust are responsible for plateau uplift. Here, we use a wide range of data that documents the long term erosion history of the plateau and a landscape evolution model to test proposed uplift histories. Model results show two plateau uplift histories that can adequately match the data. One suggests that all the plateau was uplifted rapidly ~90-100 million years ago. The other suggests two phases of uplift, one ~90-100 million years ago, and a second ~25-35 million years ago. We cannot indicate which one is correct with the data that we included, but the results have different implications for processes occurring in the deep earth.

1. Introduction

The southern African Plateau is a dominant feature of African topography, but there is still debate about when and how it formed. Topographic heights reach >3000 m, with an average elevation of ~1000 m in the predominantly low relief plateau interior. The margins of the plateau drop through higher relief regions to the coastal plain (Figure 1). The long wavelength topographic high in absence of collisional tectonism combined with Cretaceous kimberlite activity and a large low shear seismic velocity province (LLSVP) in the deep mantle below southern Africa have led many to suggest uplift related to mantle processes. Potential mechanisms contributing to uplift include lithospheric heating and modification related to kimberlite magmatism or delamination (e.g., Bell et al., 2003; Hu et al., 2018; Stanley et al., 2013; Tinker et al., 2008b), small scale convection induced when the African plate became stable with respect to the underlying mantle (e.g., Burke, 1996; Burke & Gunnell, 2008), and dynamic topography associated with the LLSVP (e.g., Braun et al., 2014; Gurnis et al., 2000; Lithgow-Bertelloni & Silver, 1998). Given that surface uplift may be related to LLSVP development, better constraints on the timing of uplift could provide additional information on the nature and development of this deep seismic anomaly and mantle processes that may cause southern Africa's anomalous elevations (e.g., Gurnis et al., 2000).

Overall, three main intervals have been proposed for when most of the uplift occurred in southern Africa (summarized in Table 1). First, the plateau may already have been elevated prior to 130 Ma at the time of Gondwana breakup due to processes that occurred prior to or associated with supercontinent breakup. Hypothesized geodynamic mechanisms to achieve uplift at this time include thermal uplift and crustal thickening due to large igneous provinces (LIPs, e.g., Cox, 1989), isostatic rebound after dynamic subsidence and deposition of the continental Karoo Basin (Pysklywec & Mitrovica, 1999), and inherited topography (Doucouré & de Wit, 2003). Most of the supporting evidence for pre-130 Ma uplift is based on the morphology of rift flank uplifts, their erosion, and models for their evolution (e.g., Gilchrist et al., 1994; Gilchrist & Summerfield, 1990; Van Der Beek et al., 2002). Second, uplift may have occurred 100-80 Ma. This timing is supported by a major pulse of continental erosion detected by thermochronology and marine sediment flux (e.g., Baby et al., 2020; Flowers & Schoene, 2010; Gallagher & Brown, 1999b; Guillocheau et al., 2012; Kounov et al., 2013; Stanley et al., 2013; Tinker et al., 2008a; Wildman et al., 2015). Many geodynamic mechanisms have been proposed to generate

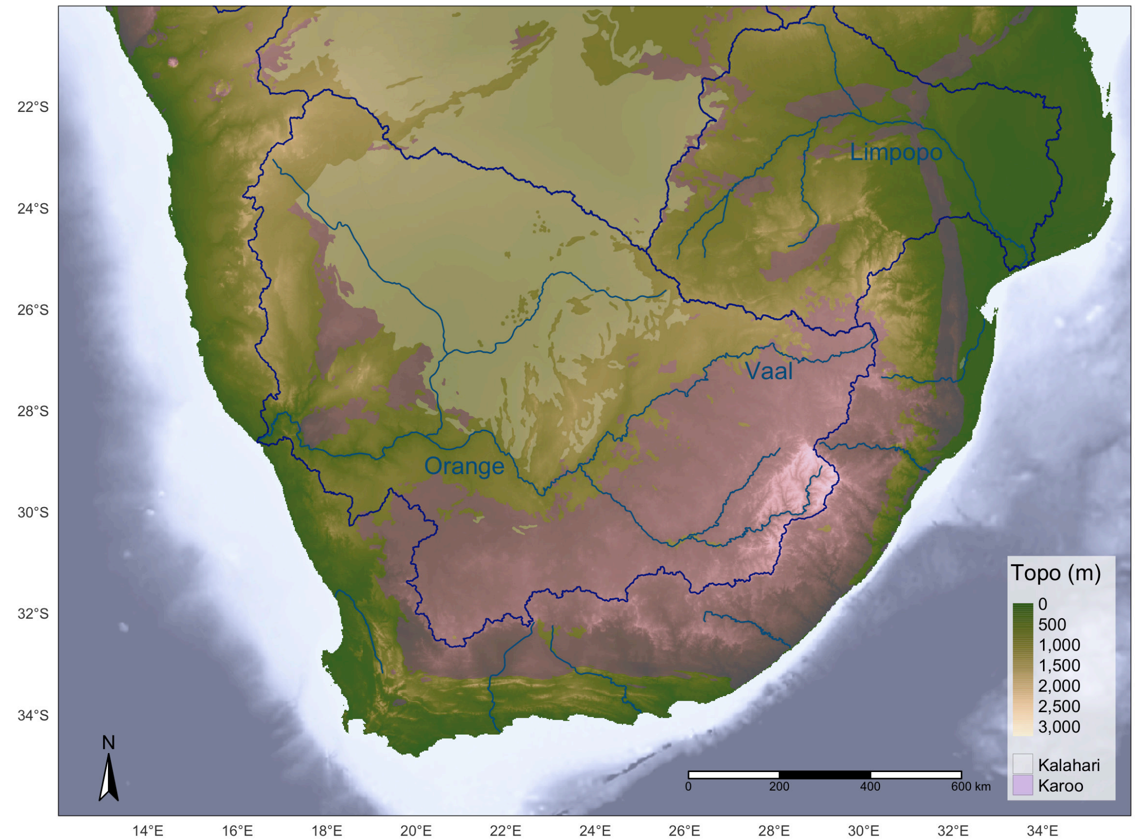

Figure 1. Topography and simplified post-300 Ma geology for southern Africa. Dark blue lines show the main drainage divides. Purple shading denotes the extent of Permian to Jurassic Karoo sedimentary basin, Jurassic Karoo lavas and sills, and early Cretaceous Etendeka Lavas, while the light shading shows the extent of thin Cenozoic Kalahari basin deposits.

plateau uplift at this time (see Table 1), but the two most commonly invoked are dynamic topography due to the LLSVP (e.g., Braun et al., 2014; Lithgow-Bertelloni & Silver, 1998) or changes in lithospheric buoyancy associated with kimberlite magmatism (e.g., Hu et al., 2018; Stanley et al., 2013; Tinker et al., 2008b). Continent-wide tilting has been shown to be important during this phase (Braun et al., 2014), and potentially caused by either motion of the African plate onto a dynamic topography high above the LLSVP (Braun et al., 2014), or delamination and/or lithospheric changes buoyancy with the east to west progression of kimberlites (Bell et al., 2003; Hu et al., 2018). Finally, uplift may have occurred after ~30 Ma. This is usually attributed to dynamic topography and small scale convection in the upper mantle (e.g., Al-Hajri et al., 2009; Burke, 1996), though others suggest that the LLSVP developed during this period (Al-Hajri et al., 2009; Gurnis et al., 2000). Evidence for Cenozoic uplift is dominantly based on mapping of planation surfaces, (e.g., Burke, 1996; Burke & Gunnell, 2008; Partridge & Maud, 1987; Paul et al., 2014; G. G. Roberts & White, 2010), river profile analysis (e.g., Paul et al. 2014; Roberts & White, 2010), or stratigraphic data (tilting and truncation of the margin, forced regressive wedges, e.g. Baby et al., 2018). Some authors (Baby et al., 2020) suggested a two steps-uplift of the southern Africa Plateau, at 93-70 (tilting of the plateau) and 25-15 Ma (Indian Ocean side only).

The timing and patterns of uplift are key for resolving the driving mechanisms, but because topographic uplift is difficult to discern directly from the continental rock record there remains discussion on how extensive surface uplift was during each of these three intervals. There are rarely direct proxies for paleoelevation, and commonly surface uplift is inferred based on the assertion that topographic uplift generates relief which triggers an erosional response that is easier to detect in the rock record. Recent work using thermochronology (Brown et al., 2014; Green et al., 2017; Kounov et al., 2013; Stanley et al., 2013, 2015; Stanley & Flowers, 2020; Wildman et al., 2015, 2016, 2017) and quantifying sediment flux to the marine basins (Baby et al., 2020; Baby, Guillocheau, Boulogne, et al., 2018; Baby, Guillocheau, Morin, et al., 2018; Guillocheau et al., 2012; Said et al., 2015) combined with extensive previous work (Belton & Raab, 2010; Brown et al., 2002; Flowers & Schoene, 2010; Gallagher & Brown, 1999a, 1999b; Kounov et al., 2009; Raab et al., 2002; Rouby et al., 2009; Tinker et al., 2008a, 2008b) now gives a fairly complete picture of the long term erosion and sedimentation history in southern Africa. Together these records show a substantial pulse of continental erosion and associated marine sedimentation in the Cretaceous with little erosion after that time. This has led many to suggest that the plateau was uplifted in the Cretaceous with limited subsequent activity (e.g., Brown et al., 2002; Flowers & Schoene, 2010; Stanley et al., 2015; Tinker et al., 2008b; Wildman et al., 2017), but the magnitude of surface uplift required to drive this erosion phase is not known. Additionally, the morphology of the landscape should contain signatures of the uplift history, and some have argued for more recent uplift of the plateau based dominantly on geomorphic observations. These include the postulated ages of geomorphic planation surfaces (e.g., Burke, 1996; Burke & Gunnell, 2008; King, 1942, 1950; Partridge et al., 2010; Partridge & Maud, 1987) as well as river profile inversion work (Paul et al., 2014; G. G. Roberts & White, 2010; Rudge et al., 2015). However, the time or rate of formation of some of these geomorphic features is difficult to constrain.

Surface process models that focus on some or all of the landscape can be used to derive more quantitative estimates of how topographic change relates to erosion history and geomorphic features. Previous work linking topography and AFT data from the southwest coast indicated the existence of a pre-breakup drainage divide similar to the present-day divide in this area (Van Der Beek et al., 2002). Block landscape models aimed at reproducing the sediment flux to the west coast marine basins showed that continent-scale tilting during early Late Cretaceous uplift was necessary to reproduce the observations (Braun et al., 2014). Additional modelling of a generic continent subjected to a propagating wave of dynamic topography argued that the modelled sedimentary architecture was consistent with Cretaceous sedimentary archives from southern Africa (Ding et al., 2019). Modelling efforts focused on river profile shape have taken this approach a step further by comparing modeled and observed river profiles to invert for uplift histories that suggest that the high topography was developed in the last 30-40 Ma (Paul et al., 2014; G. G. Roberts & White, 2010; Rudge et al., 2015). This is an interesting methodology because it allows the systematic exploration of a wide range of uplift parameters, but the absolute timing of the uplift histories it yields depends on an assumed value for rock erodibility, which is difficult to constrain. All of these methods have only focused on one main piece of the erosion history or landscape, yielding important insights into aspects of the southern African topographic history but leading to incomplete and sometimes conflicting results between modeling approaches.

Timing	Geodynamic Mechanism	Evidence
Before or during Gondwana breakup (> 130 Ma)	▪ Thermal uplift and crustal thickening associated with LIP activity (Cox, 1989) ▪ Isostatic rebound after dynamic subsidence and deposition of the Karoo basin (Pysklywec & Mitrovica, 1999) ▪ Inherited Paleozoic topography (Doucouré & de Wit, 2003) ▪ Flexural uplift from far field plate stresses (A. E. Moore, 1999; A. E. Moore et al., 2009)	▪ Major phase of cooling in AFT thermochronology studies around the margins just after rifting (Brown et al., 1990, 2002; Gallagher & Brown, 1999a; Tinker et al., 2008b; Wildman et al., 2015, 2016) ▪ Models of escarpment retreat developed in S. Africa suggest some topography at breakup (Gilchrist et al., 1994; Gilchrist & Summerfield, 1990) and a pre-existing topographic divide (Van Der Beek et al., 2002) ▪ Radial drainages around LIPs (Cox, 1989)
Mid-Cretaceous (110-80 Ma)	▪ Dynamic topography due to the LLSVP in the deep mantle (Braun et al., 2014; Lithgow-Bertelloni & Silver, 1998) ▪ Changes to the lithospheric density structure (Bell et al., 2003; Stanley et al., 2013), long lived plume tails (Nyblade & Sleep, 2003), and/or delamination (Hu et al., 2018) associated with kimberlite magmatism ▪ Pressure driven flow in the asthenosphere (Colli et al., 2014) ▪ Flexural uplift from far field plate stresses (Moore, 1999; Moore et al., 2009) ▪ Agulhas LIP off the S coast at ~90 Ma (M. de Wit, 2007)	▪ Phase of cooling seen in AFT (Brown et al., 2002; Gallagher & Brown, 1999a, 1999b; Kounov et al., 2009; Tinker et al., 2008b; Wildman et al., 2015) and AHe (Flowers & Schoene, 2010; Kounov et al., 2013; Stanley et al., 2013, 2015; Stanley & Flowers, 2020; Wildman et al., 2017) ▪ Major pulse of sediment delivered to the marine basins off the western and southern coasts (Baby et al., 2020; Guillocheau et al., 2012; Rouby et al., 2009; Tinker et al., 2008a). ▪ Geometric evidence from offshore forced regressive wedges, margin tilting, and incised valleys (Baby et al. 2020)
Mid- to Late Cenozoic (<35 Ma)	▪ Small scale convection in the upper mantle due to the slowing of African plate at ~30 Ma (Burke, 1996; Burke & Gunnell, 2008; Burke & Wilson, 1972) ▪ Dynamic topography due to density variations in the upper mantle and/or the LLSVP (Al-Hajri et al., 2009; Gurnis et al., 2000; Lithgow-Bertelloni & Silver, 1998; Moucha & Forte, 2011; Paul et al., 2014; Winterbourne et al., 2009) Flexural uplift from far field plate stresses (Moore, 1999; Moore et al., 2009)	▪ Large scale correlation of geomorphic surfaces (Burke & Gunnell, 2008; King, 1942; Partridge & Maud, 1987) ▪ River profiles and models of their formation through time (Paul et al., 2014; G. G. Roberts & White, 2010; Rudge et al., 2015) ▪ Terraces on the lower Orange River (Dauteuil et al., 2015) ▪ Geometric evidence from offshore forced regressive wedges and margin tilting (Baby et al. 2020) ▪ Inferred cooling phase on the southern coast (Green et al., 2017)

Table 1. Proposed geodynamic mechanisms and evidence for proposed stages of uplift

Here we aim to take advantage of the many datasets quantifying the erosion history of southern Africa and combine them with topographic metrics to explore how much uplift occurred during each of the three proposed periods of plateau development using landscape evolution model inversions. By using thermochronology dates, marine sediment flux volumes, and topography we aim to quantify the surface uplift histories that are most compatible with all the observations. To do this, we use a highly efficient forward landscape evolution model, FastScape (Braun & Willett, 2013), to predict erosion and topography from a wide range of uplift histories and erosional parameters. Model outputs are directly compared with observations, and we use an inversion optimization scheme to isolate the uplift histories that best match the data. Resulting good fit histories give quantitative estimates of uplift magnitudes and rates through time that are compared to proposed geodynamic mechanisms for uplift. Results yield insights into the links between topographic change and erosion in southern Africa that could be compared directly with the outputs of geodynamic models in the future.

2. Background

2.1 Geomorphic and Geologic setting

Combined with the eastern African Plateau and anomalously shallow bathymetry in the southeast Atlantic Ocean, southern Africa forms a part of the "African superswell" (Nyblade & Robinson, 1994) of high topography and bathymetry. Unlike the eastern African Plateau and the other topographic swells in north and central Africa, southern Africa does not have active volcanism. It forms a broad (>1200 km wide) plateau with the highest elevations around the rim of the plateau forming what has been termed the "great escarpment" (Fig 1). The escarpment sits generally 100-200 km inboard of the coast and is often interpreted as a resulting from the retreat of set of flexural rift shoulders (e.g., Braun, 2018; ten Brink & Stern, 1992; Gilchrist et al., 1994) that separates the higher relief, more heavily eroded coastal plains from the plateau interior. At present, the interior of the plateau is almost entirely drained by the west-draining Orange River system. Evidence from much higher sediment flux rates on the west coast (e.g., Baby et al., 2020; Guillocheau et al., 2012; Tinker et al., 2008a) and the locations of detrital diamond sources (Bluck et al., 2005; Nakashole et al., 2018; Phillips et al., 2018; Phillips & Harris, 2009) show that the plateau has been west-draining since Gondwana breakup. Drainage reconstructions suggest some reorganization of plateau drainage since the Cretaceous, but most suggest the dominance of large, west-draining river systems (R. Dingle & Hendry, 1984; Partridge & Maud, 1987; Stevenson & McMillan, 2004; M. C. J. de Wit, 1999).

Geologically, southern Africa is a continental shield composed of dominantly Precambrian lithosphere. The Archean Kaapvaal and Zimbabwe cratons are sutured by the Archean to Paleoproterozoic Limpopo Belt and surrounded by several other Proterozoic mobile belts. This crystalline basement is overlain by several locally preserved Precambrian sedimentary and volcanic sequences. In the south, the Paleozoic Cape Supergroup was folded into the Cape Fold Belt (~275 Ma to ~250 Ma, Hansma et al., 2016). Much of the Cape Fold Belt consists of quartzites that are resistant to erosion (Scharf et al., 2013). As a whole these Precambrain and Paleozoic rock units are relatively resistant to erosion.

The Karoo sedimentary sequences were deposited from ~300 Ma to ~180 Ma. They once covered much of southern Africa with substantial thickness still preserved today (Fig 1). Their deposition was partly contemporaneous with the development of the Cape Fold Belt and in places they are deformed by this event (Linol & De Wit, 2016). These sediments were deposited either in a foreland basin related to this orogeny (Catuneanu et al., 2005) or due to dynamic subsidence induced by subduction to the south (Pysklywec & Mitrovica, 1999). The base of the Karoo Supergroup consists of marine glacial sediments (Dietrich & Hofmann, 2019) and turbiditic to continental deposits (Catuneanu et al., 2005; Johnson et al., 1996). Sedimentation terminated with the eruption of the ~183 Ma basalts of the Karoo Large Igneous Province (LIP) (Duncan et al., 1997; Jourdan et al., 2008). In addition to the basalts, an extensive network of dolerite sills was emplaced within the entire Karoo sequence, concurrent with the eruption of the basalts at the surface (Svensen et al., 2012). The maximum preserved thickness of the Karoo Supergroup is up to 6 km (Scheiber-Enslin et al., 2015), with up to 1.7 km of basalt preserved in the Lesotho remnant (Marsh et al., 1997). The clastic sediments of the Karoo sequence are much less resistant to erosion than the underlying Precambrian rocks and Cape Fold Belt (e.g., Braun et al., 2014).

Post-Karoo units include the relatively thin poorly-dated Kalahari sediments (Early Cretaceous? to Cenozoic) in the north, the igneous rocks of the ~132 Ma (Renne et al., 1996) Etendeka LIP in western Namibia and South Africa, and many Cambrian to Paleogene kimberlites. There are two major pulses of kimberlite magmatism in the Jurassic through Cretaceous, with pulses peaking at ~90 Ma and ~120 Ma (Jelsma et al., 2004).

2.2 Constraints on the erosion history of southern Africa

2.2.1 Offshore constraints from stratigraphy

Terrigenous sedimentary flux shed off the continent has been quantified for the western and southern margins of southern Africa based on seismic lines and borehole data (Baby et al., 2020; Baby, Guillocheau, Boulogne, et al., 2018; Baby, Guillocheau, Morin, et al., 2018; Guillocheau et al., 2012; Rouby et al., 2009; Tinker et al., 2008a). This includes quantifying the siliciclastic component by correcting for in-situ carbonate production and porosity (Baby et al., 2020; Baby, Guillocheau, Boulogne, et al., 2018; Baby, Guillocheau, Morin, et al., 2018; Guillocheau et al., 2012). The Orange River presently drains most of the southern African Plateau, such that much of the sediment removed from the landscape is deposited in the Orange River Basin. There is also fairly limited on-shore sediment storage in the Orange River drainage, with no large continental basins, making this a good location for source to sink studies. The sedimentary sequence in the Orange Basin basin records two periods characterized by high sedimentary volumes and accumulation rates in Early and Late Cretaceous times, with particularly high depositional volumes in the Orange Basin between 93.5 and 81 Ma (Baby, Guillocheau, Morin, et al., 2018). The interval between 130 and 100 Ma as well as the Cenozoic period are characterized by low sediment volumes and accumulation rates, though there is a slight uptick in rates in the southern part of the margin since 11 Ma (Fig. 2, Baby, Guillocheau, Morin, et al., 2018; Guillocheau et al., 2012). The basins off the southern and eastern coasts show much lower volumes of sediment but with a similar pattern: high accumulation rates in the Early and Late Cretaceous, followed by much lower sediment volumes in the Cenozoic (Fig. 2, Baby, Guillocheau, Boulogne, et al., 2018; Braun et al., 2014; Tinker et al., 2008a). Together these observations suggest intervals of increased erosion and sediment transport to the basins surrounding southern Africa in the Early Cretaceous just following rifting and in the Late Cretaceous ~100-65 Ma, with increased sedimentation rates first appearing in the Orange River Basin ~95-90 Ma.

The sedimentary record of both the Indian (Baby, Guillocheau, Boulogne, et al., 2018) and Atlantic (Baby, Guillocheau, Morin, et al., 2018) Margins show evidence for two phases uplift at around 93-70 Ma and 25-15 Ma. Evidence comes from margin tilting and truncation, forced regressive wedges recording a relative sea level fall with an amplitude higher than 100m/Ma and incised valleys (see Baby, Guillocheau, Boulogne, et al., 2018 for a discussion). The stratigraphic record (Braun et al., 2014; Baby, Guillocheau, Boulogne, et al., 2018; Baby,

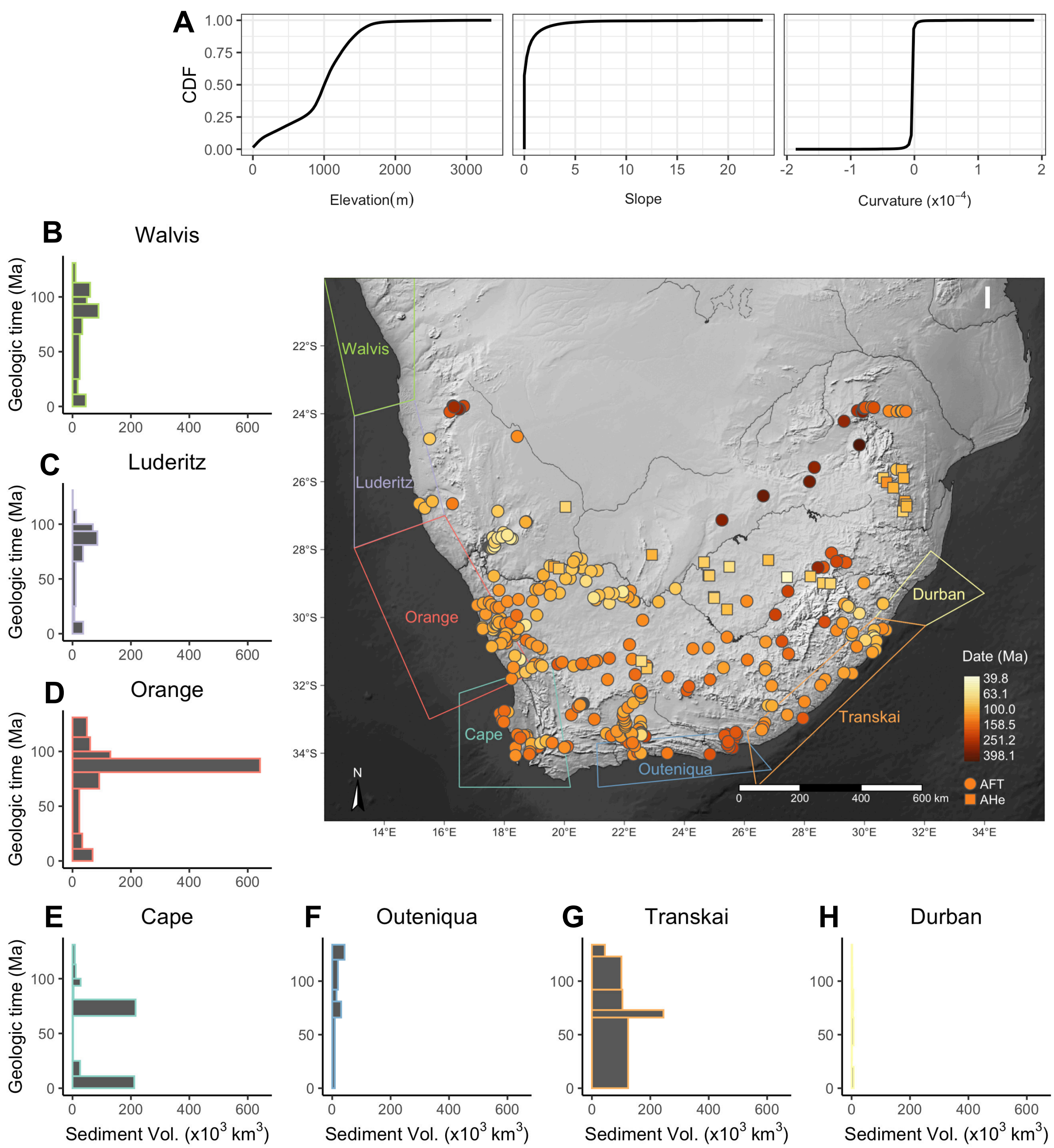

Figure 2. Data included in inversion modeling. A) Cumulative density functions (CDF) for present day elevation, slope, and curvature from southern Africa derived from the ETOPO1 dataset (Amante & Eakins, 2009). B-H) Sediment volumes deposited over time in the marine basins surrounding southern Africa (Baby et al., 2020). I) Shaded relief map showing the locations of low temperature thermochronology dates with color denoting age (Brown, 1990; Brown et al., 2002, 2014; De Wit, 1988; Flowers & Schone, 2010; Green et al., 2017; Kounov et al., 2009, 2013; Raab et al., 2002; Stanley et al., 2013; 2015; Stanley & Flowers, 2020; Tinker et al., 2008; Wildman et al., 2015, 2016, 2017)

252

Guillocheau, Morin, et al., 2018) indicates margin uplift and tilting of the Southern African Plateau, starting to the east (Maputaland to Durban Margin) at 93 Ma and ending to the west (Orange to Olifant Margin) at 81-70 Ma. After a period of no deformation (70-35 Ma), significant uplift started again along the Durban to Maputaland Margin (25-15 Ma) and earlier (35 Ma) along the Zambezi Margin (Ponte et al. , 2019).

2.2.2 Onshore constraints from thermochronology

Apatite fission-track (AFT) and (U-Th)/He (AHe) thermochronology are dating techniques that track the cooling and heating of rocks through the upper ~1-6 km of crust and can be used to constrain the long term burial and erosion of a region. AHe is sensitive to temperatures of ~30-90°C (Farley, 2000; Flowers et al., 2009; Shuster et al., 2006). Assuming a typical cratonic geothermal gradient of 20°C/km, AHe can be used to detect erosion in the upper ~0.5-3.5 km of crust. AFT is sensitive to somewhat higher temperatures of ~60-110°C (Green et al., 1986) or ~2-4.5 km depth assuming the same cratonic gradient. Many studies have used low temperature thermochronology to constrain the long-term erosion histories in southern Africa.

The majority of studies have used AFT on the high relief eastern (Brown et al., 2002), southern (Green et al., 2017; Tinker et al., 2008b) and western (Gallagher & Brown, 1999b; Kounov et al., 2009, 2013; Wildman et al., 2015, 2016) passive margins of the plateau (Fig 2). These studies show two periods of accelerated erosion in the Cretaceous, the first at ~150-120 Ma following continental breakup and the second at ~100-70 Ma. This work also suggests limited Cenozoic erosion, though Green et al. (2017) suggest an episode of burial and erosion of parts of the Southwest Cape during the Cenozoic. AHe data across the eastern plateau escarpment also detects a cooling phase at ~100 Ma and limits Cenozoic erosion to <750 m (Flowers & Schoene, 2010). AHe data across the interior of the plateau record greater spatial variability than the plateau edges. In the Proterozoic basement of the southwestern plateau AHe data indicate an intensified erosion phase from ~110-90 Ma, whereas in the Archean basement of the central plateau a wave of erosion migrated eastward from ~120 Ma to <60 Ma (Stanley et al., 2013, 2015; Stanley & Flowers, 2020)[Stanley et al., 2013, 2015, 2020], and the central part of the Kaapvall Craton shows limited erosion since before the breakup of Gondwana (Wildman et al., 2017). These results also suggest limited Cenozoic erosion of ~1 km or less.

Cosmogenic nuclide derived erosion rates suggest that erosion rates on both the plateau surface and the coastal plain have been slow over the last few Myr. Most erosion rates, both catchment averaged and bedrock, are <10 m/Myr (Bierman et al., 2014; Chadwick et al., 2013; Cockburn et al., 1999, 2000; Decker et al., 2013; Dirks et al., 2016; Fleming et al., 1999; Kounov et al., 2007; Makhubela et al., 2019; Scharf et al., 2013), one to two orders of magnitude lower than thermochronologically derived rates for the Cretaceous. However, several studies focused around river channels suggested slightly higher denudation rates (12 to 255 m/Ma) highlighting some potential landscape variability (Erlanger et al., 2012; Keen-Zebert et al., 2016).

2.2.3 Onshore constraints from geological observations

Early geomorphologists described and correlated a number of geomorphic surfaces across the southern African landscape that were attributed to cycles of uplift and denudation (e.g., Dixey, 1955; King, 1942, 1950; Partridge & Maud, 1987). Age assumptions for these surfaces suggest plateau uplift in the Cenozoic (Burke, 1996; Burke & Gunnell, 2008; Partridge & Maud, 1987), but arguments used for dating are quite poor and the uplift scenario is questionable. Recent work suggests that the surfaces in the plateau interior are mid to Late Cretaceous in age based on cross cutting kimberlites (Baby, 2017). Pediments and wave cut platforms on the continental margins are thought to be younger (<25 Ma, Baby, 2017). In the lower Orange River Valley, these surfaces and alluvial terraces were used to argue for >200 m of uplift of this region in the Cenozoic (Dauteuil et al., 2015).

Reconstructed thicknesses of the Karoo Basin can help constrain total erosion magnitudes since ~180 Ma. The amount of material denuded across the main Karoo basin on the plateau surface is estimated at ~0.5-3 km of material (Hanson et al., 2009), but vary based on location, reconstruction method, and the proposed thinning rates for the units (Hanson et al., 2009; Hawthorne, 1975; Johnson et al., 1996). Similar efforts at reconstructing stratigraphic thicknesses on the southern margin suggest a range of erosional magnitudes from 4-11 km, in line with AFT data (Richardson et al., 2017). Kimberlites can contain crustal xenoliths that record the sedimentary cover present at the time of eruption and provide additional information on erosional timing. Upper crustal xenoliths from kimberlites suggest that the Karoo sedimentary section in the central plateau was removed in the Cretaceous in a west to east pattern that is consistent with the AHe data (Hanson et al., 2009; Stanley et al., 2015). In addition, crater lake sediments preserved in the ~75-65 Ma kimberlite pipes in the western Plateau suggest that this area has seen very limited erosion since that time (A. Moore & Verwoerd, 1985; Scholtz, 1985; Smith, 1986).

3. Modelling methods

3.1 Modelling strategy and data

We seek to test the three proposed intervals for the rise of the southern African plateau using the breadth of erosion and sedimentation data that is now available here. To do this we use a large-scale landscape evolution model to predict thermochronology dates, sediment fluxes, and topography from different uplift inputs. We explore which parameter sets fit the observations best using inversion methods combined with an optimization algorithm. The parameter space is too large to sample in its entirety, so we use the neighborhood algorithm (NA, for full description see Sambridge, 1999), to guide a total of 300,000 model runs varying 11 parameters (Table 2). We then compare model results to three different types of observations: thermochronology dates, marine sediment flux volumes, and topographic metrics.

The thermochronology data include 363 published AFT dates from Precambrian basement and Karoo sedimentary rocks (Belton & Raab, 2010; Brown et al., 1990, 2002, 2014; Green et al., 2017; Kounov et al., 2009, 2013; Raab et al., 2002; Tinker et al., 2008b; Wildman et al., 2015, 2016, 2017) and 29 average AHe dates from Precambrian basement and Cretaceous kimberlites and mafic rock samples (Flowers & Schoene, 2010; Stanley et al., 2013, 2015; Stanley & Flowers, 2020). The full data table can be found in the supplementary materials Table S1. Samples span from across southern Africa between 23.5°S and 36°S and cover both the coastal margins and the plateau interior, though there is more data from the coastal regions (Fig 2).

The sediment flux data comes from volume estimates in seven marine basins on the western and southern coasts of southern Africa (Fig 2). These volumes were calculated from seismic constraints and borehole observations (Baby et al., 2020; Baby, Guillocheau, Boulogne, et al., 2018; Baby, Guillocheau, Morin, et al., 2018). They are estimates of the terrestrially derived sediment and have been corrected for in-situ carbonate production, porosity, and compaction. Tables of the sedimentary volumes and basins are located in the supplement (Table S2).

The present-day topography is derived from the ETOPO1 one arc minute global topographic and bathymetric dataset (Amante & Eakins, 2009). Topography ranges from sea level to 3376 m elevation, with a median elevation of 1037 m (Fig 2).

3.2 Forward model setup

3.2.1 Model setup and uplift

The landscape model runs from 145 Ma to present with timesteps of 1 Myr. Parameterization of the model allows for topographic development corresponding to the three main phases that have been proposed for uplift of the Kalahari Plateau: 1) Initial topography that represents topography formed prior to Gondwana breakup, 2) A phase of uplift and continental tilting in the Cretaceous, and 3) A phase of block uplift in the Cenozoic (Figure 3, Table 1). The magnitude and time of uplift during these phases are variable within the inversion (Table 2).

The initial topography is the first phase of uplift input, representing any plateau development that occurred prior to or during Gondwana breakup. All models start with 5% of today's topography (0-150 m) to seed the drainage basins. This is then uplifted uniformly within the first timestep by an additional plateau height h_0 which induces a flexural response at the margins, mimicking rifted margin topography (Figure 3, Table 2). We seed the drainage basins to reflect the current basins because the geologic record indicates that large, west-draining river systems have been persistent in southern Africa since Gondwana breakup (e.g., M. C. J. de Wit, 1999). This westward draining nature of the plateau is important for determining where sediment is routed, and we found that such a drainage geometry was difficult to create spontaneously. 5% of today's topography is sufficient to setup a west draining geometry, but low enough magnitude that it can be easily disrupted by uplift imposed later in the model.

In the Cretaceous we impose a phase of continental tilting that initiates in the east at a time t_{init}. It tilts linearly to the west, reaching a maximum height of h_{tilt} 5 Myr after uplift initiates (Fig 3, Table 2). The continent remains tilted for a duration of time t_{tilt}, at which point uplift begins from the west reaching the same height and a flat uplift after 5 Myr (Fig 3). The continent then retains this dynamic uplift for the rest of the model run. We chose this continental tilting shape for the Cretaceous uplift phase because previous modeling (Braun et al., 2014) showed that this was important for producing the large pulse of sediment observed in the basins off the west coast. Additionally, we found that the tilting geometry was best for preserving a large-west

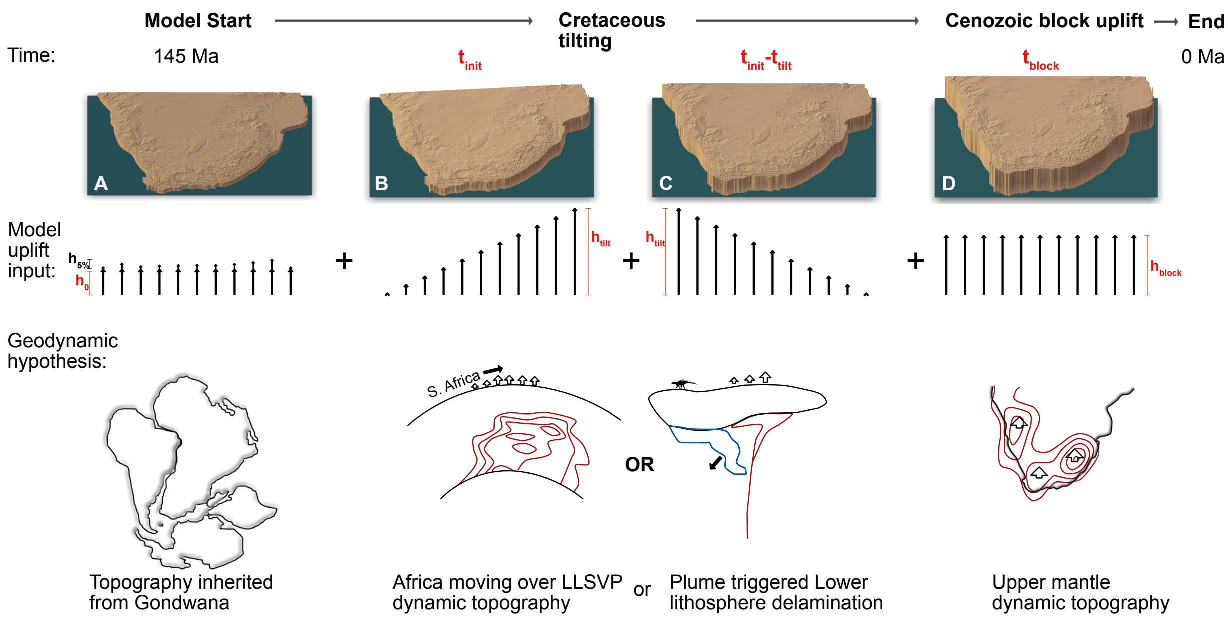

Figure 3. Schematic diagram of uplift imposed on the model through time. Parameters in red are variable in the inversion, while black are fixed. During the first time step (A), an uplift of height h_o plus 5% of present day topography is imposed. At time t_{init} (B) a linear tilt is imposed as a vertical stress at the base of the model, and after t_{tilt} an opposing tilt to flatten the continent is imposed (C). Finally, at t_{block} a vertical stress at the base of the model is imposed to create an additional height of h_{block} (D). It should be noted that uplifts that are imposed as a vertical stress may produce magnitudes of rock uplift and erosion higher than the uplift amount due to isostatic feedback. Times are shown in geologic time. Bottom panels show cartoons depicting geodynamic hypotheses being tested at each stage. Uplift at model start represents topography inherited from prior to Gondwana breakup. Cretaceous tilting could be due to movement of Africa over a dynamic topography high due to the lower mantle LLSVP or lower lithosphere delamination triggered by kimberlite magmatism. Cenozoic uplift could be due to upper mantle buoyancy, perhaps denoted by present day free air gravity anomaly highs (after Winterbourne et al., 2009). See Table 1 for more explanation.

376

draining drainage basin geometry while many other uplift shapes we tested disrupted this drainage network.

Finally, in the Cenozoic, at a time t_{block}, a phase of dynamic block/uniform uplift is imposed with a magnitude h_{block} (Fig 3, Table 2). Once its maximum value is reached, the uplift is maintained until the end of the model run.

The model domain ranges from 20°S to 35°S and 12°W to 36°W and is discretized on a 1 arc-second grid. For simplicity, base level remains fixed at the present-day coastlines throughout the model run, and the northern boundary is a reflective, no-flux boundary. The model starts with a uniform, 2 km thick softer layer representing the Karoo basin sediments and basalts overlying a harder layer representing the Precambrian basement.

Variable Parameter	**Units**	**Value Range**	**Hybrid best fit**	**Cretaceous best fit**
K_f: Erosivity	$m^{0.2}/yr$	10^{-7} to 10^{-4}	$3.387x10^{-6}$	$7.545x10^{-5}$
ε_c: Threshold for erosion	m/yr	10^{-5} to 10^{-2}	$1.111x10^{-4}$	$9.544x10^{-3}$
T_{max}: Temperature at base of 120 km thick model lithosphere	°C	2400 to 5000	4430	4987
R_k: Ratio of thermal diffusivity between 2km thick Karoo sedimentary cover and underlying basement		0.3 to 1	0.307	0.310
R_D: Ratio between volume of material eroded and volume of material deposited in the marine basins		1 to 5	3.625	3.005
h_0: height of initial base plateau in first time step	m	200 to 2000	233.2	206.1
t_{init}: Geologic time when uplift and tilting initiates in the east	Ma	120 to 75	94.72	97.50
h_{tilt}: Magnitude of Cretaceous tilting	m	200 to 3000	481.8	1414.5
t_{tilt}: Duration of time continent remains tilted before uplift initiates in the west	Myr	5 to 35	21.86	5.905
t_{block}: Geologic time of second phase of block uplift	Ma	40 to 0	33.09	22.19
h_{block}: amount: magnitude of second phase of uplift	m	0 to 2000	824.2	0.731

Table 2A – Variable parameters in inversion model, their ranges, and their values from the best fit models from the Cretaceous and Hybrid Scenarios

Fixed Parameter	Units	Value	Justification
n: Slope exponent in stream power law		1	Literature values range from 0 to 4, n=1 chosen for numerical efficiency
m: Drainage area exponent in stream power law		0.4	Literature values range from 0 to 2, ratio of m/n derived from slope-area relationships in natural landscapes ranges from 0.35-0.6 (Kirby & Whipple, 2012; Whipple, 2004; Whipple & Tucker, 1999)
T_e: Elastic thickness	km	20	Effective elastic thickness estimates for southern Africa range from ~10 km near the coasts to >70km in the cratonic interior (Doucouré et al., 1996; Pérez-Gussinyé et al., 2009). We have chosen a value representative of the continental margins because flexural effects are most important to the landscape there.
t_{up}: time period over which each dynamic uplift stage is imposed	Myr	5	It is geologically unreasonable for uplift to occur instantaneously
Karoo layer thickness	km	2	Soft layer representing sediments and basalt overlying basement that can also have different thermal diffusivity.
Karoo layer erosivity	$m^{0.2}/yr$	30(K_f)	Braun et al. (2014) demonstrated that a soft layer was important for reproducing the Cretaceous sediment pulse
E: Young's modulus	GPa	$1x10^{11}$	
ν: Poisson's ratio		0.25	
ρ_c: crustal density	kg/m^3	2750	
ρ_a: asthenospheric density	kg/m^3	3300	
κ: thermal diffusivity of basement	m^2/yr	25	
Lithospheric thickness	km	120	
Kinetic model for apatite fission track annealing			Crowley et al. (1991)
Kinetic model for He diffusion in apatite			Farley (2000)

Table 2B – Fixed parameter values and justification.

3.2.2 The landscape evolution model

The landscape evolution model solves the basic stream power model for bedrock river incision (Howard & Kerby, 1983),

$$\frac{\partial h}{\partial t} = U - max(0,\ K_f S^n A^m - \varepsilon_c) \qquad (1)$$

where h is the height of the topography, t is time, U is uplift rate, S is slope, A is drainage area, K_f is the erosion efficiency scaling parameter, m and n are constants, and ε_c is an erosion threshold. Equation (1) is solved by the FastScape algorithm (Braun & Willett, 2013). FastScape is a very efficient, first order, implicit, finite difference algorithm for solving the stream power equation that makes it possible to run many forward models rapidly enough to complete inversions. The values of K_f, m, and n are not well constrained but depend dominantly on climate, lithology, and hydrology. We use standard values of n=1 and m=0.4 and allow K_f to vary over several orders of magnitude between 10^{-7} and 10^{-4} $m^{0.2}$/yr. The top 2 km of the model is a layer of soft material representing the Karoo basin where K_f for the layer is 30 times the value of K_f for the underlying material. All parameter values and their justification can be found in Table 2 (see Croissant & Braun, 2014, for a more thorough discussion of the values of the erosional parameters). The introduction of the erosion threshold, ε_c with units of m/yr, implies that some base level of stream power is needed to erode the landscape. ε_c is also allowed to vary over several orders of magnitude (Table 2). Flow is routed using a D8 grid connectivity, and local depressions are filled using the algorithm of Cordonnier et al. (2019). We do not include a model for hillslope processes because they cannot be adequately represented at the scale of our model (i.e., grid resolution of 1x1 km). This is a highly simplified description of erosion, and unlikely to capture the true complexity of erosion processes across the southern African landscape. However we feel it is sufficient for comparison at the scale of our model and data types we have incorporated.

We compute the flux of sediment leaving the continent along various sections of the continental margin corresponding to major depocenters as shown in Figure 2. We introduce a deposition ratio, R_D, which multiplies the eroded flux to produce a depositional flux into the marginal basins that is compared to observed fluxes. This ratio accounts for imbalances in the amount of material eroded and deposited that could be caused by processes such as chemical denudation or transport of material away from the depocenter.

The LEM is coupled to an isostatic model that includes flexure of a thin elastic plate:

$$D\frac{\partial^4 U}{\partial x^4} + D\frac{\partial^4 U}{\partial y^4} + D\frac{\partial^4 U}{\partial x^2 y^2} \ = \ \Delta\rho g U + \rho_c g \Delta h + \ \sigma_{DT} \qquad (2)$$

where D is the flexural rigidity, ρ_c is the crustal density, $\Delta\rho$ is the density difference between ρ_c and the asthenospheric density, and σ_{DT} is an imposed basal stress that could represent viscous stress from mantle flow or an isostatic response from delamination of the lithospheric mantle. D is related to Young's modulus (E), the elastic thickness (T_e) and Poisson's ratio (ν):

$$D = \frac{ET_e^3}{12(1-\nu^2)} \quad (3)$$

The flexure equation is solved using the Fast Fourier Transform method in the spectral domain on a fixed grid using methods similar to Nunn and Aires (1988).

Uplift is imposed as a vertical stress field along the base of the lithosphere through the flexural-isostatic model (equation 2) as σ_{DT}, where σ_{DT} is the stress required to lift the surface topography to the imposed height. In this setup, surface erosion results in the rebound of surface topography such that the weight of the surface topography remains equal to the basal load. This can continue until the deflection at the base of the crust is sufficient to balance the load.

3.2.3 Thermal Model

A 1D thermal model is coupled to the landscape model to predict cooling dates from the modeled erosion history for comparison with the observed data. For each location where a predicted cooling date is needed, the erosion rate is stored for each time step and used to generate an exhumation history at the end of the model run. These erosion rates are then used to solve the 1D heat equation:

$$\frac{\partial T}{\partial t} + \dot{E}\frac{\partial T}{\partial z} = \kappa\frac{\partial^2 T}{\partial z^2} + \frac{H}{c} \quad (4)$$

where c is the heat capacity, $\dot{E}$ is the erosion rate, κ is the thermal diffusivity, and H is the heat production by radiogenic elements. The implementation in the model also allows for layers with differing thermal diffusivities, and their thicknesses are adjusted throughout the model run to account for their erosion. The solution is used to compute time-temperature paths and predict dates for thermochronological systems (Braun et al., 2006).

The top and base of the models at fixed temperatures, with the surface at 15°C and T_{max} at the base of a 120 km thick lithosphere which correspond to surface geothermal gradients between ~20 and 42°C/km. The thermal diffusivity of the soft layer at the top of the model representing the Karoo sedimentary sequence can vary as a ratio of the basement thermal diffusivity, R_K, allowing for a thermal blanketing effect of up to 3 times (Table 2).

3.3 Inversion methods

We use the NA optimization (Sambridge, 1999) to guide the sampling of the large parameter space. At the start of the inversion, 10,000 random sets of parameters are selected from within the specified ranges (Table 2), and a forward model is run with each parameter. For each model, a misfit that measures how well the predicted values match the observed values is calculated. For each subsequent iteration of 1000 runs, the NA preferentially samples from areas of the parameter space with lower misfit values, while still casting a wide net (see Sambridge, 1999, for details).

The construction of a misfit function that can assign a single numerical value of how well each forward model fits the observations is central to the inversion method, however combining assessments of different data types is nontrivial. We first compute an individual misfit for each separate data type, and then we combine these into a single misfit value for the model run.

For the topographic metrics, the misfit is calculated by comparing the distributions of the predicted and observed topography using the two sample Kolmogorov–Smirnov (KS) statistic. We compare the distributions of present-day topographic height, slope, and curvature with those from our model results. We use cumulative distribution functions (CDFs) for each of these metrics calculated at the same spatial scale as the model resolution. We compare CDFs rather than directly comparing the topography because it is unlikely that the model will replicate specific features of the model (such as exact locations of valleys and mountain tops) but should be able to replicate broader characteristics of the topography. The KS statistic measures the distance between the predicted and observed distribution, yielding a value between 0 (for identical distributions) and 1 (for distributions that do not overlap). We calculate three individual misfits, M_{height}, M_{slope}, and M_{curve} that are the KS statistic for the comparison between the predicted and observed topographic height, slope, and curvature distributions.

Terrigenous sediment flux volumes have been calculated for a number of time periods in seven basins for a total of 50 volumes (Baby et al., 2020; Baby, Guillocheau, Boulogne, et al., 2018; Baby, Guillocheau, Morin, et al., 2018; Figure 2, Table S2). If N is the total number of volume calculations, the misfit for the flux, M_{flux}, takes the form of the square-root of the L_2-norm of the weighted difference between the predicted ($V_{i,pred}$) and observed ($V_{i,obs}$) volumes for the volume from each time period:

$$M_{flux} = \frac{1}{N}\sqrt{\sum_{i=1}^{N}\frac{(V_{i,pred} - V_{i,obs})^2}{\sigma_{avg}{}^2}}$$

where σ_{avg} is the average uncertainty across all the flux calculations ($13.7\text{x}10^{12}$ m^3). M_{flux} can range from 0, for V_{pred} equal to V_{obs}, to very large when V_{pred} is very different from V_{obs}. Values of $M_{flux} < 1$ indicate that the predicted values match the observed values within the average uncertainty.

The misfit for the thermochronology data, M_{thermo}, takes a similar form to the flux misfit:

$$M_{thermo} = \frac{1}{N}\sqrt{\sum_{i=1}^{N}\frac{(a_{i,pred} - a_{i,obs})^2}{\sigma_{i,obs}{}^2}}$$

where $a_{i,pred}$ is the predicted thermochronologic date for each location from the model run, $a_{i,obs}$ is the observed thermochronologic date at that location, and $\sigma_{i,obs}$ is the uncertainty associated with that date. N is the total number of thermochronologic dates included in the model, in this case 392 (Fig 2; table S1). In most situations the cooling dates for low temperature thermochronometers are expected to vary systematically with elevation (e.g., Braun, 2002). Because we cannot expect the model to reproduce the exact characteristics of the landscape, $a_{i,pred}$ is taken from the location within a 20km radius that is closest in elevation to the observed date. M_{thermo} also ranges from 0 for an exact match between the predicted and observed dates to very large for a poor match with $M_{thermo}<1$ indicating that the model predictions match the observations within uncertainty.

The total misfit, M, for the model run is the sum of the five individual misfits for the different data types:

$$M = M_{height} + M_{slope} + M_{curve} + M_{flux} + M_{thermo}$$

The misfit used to guide the parameter search in the inversion is therefore a combination of how well the model fits the combination of data types. It should be noted that the form of the misfit and how the different misfit types are weighted has a strong effect on the inversion results.

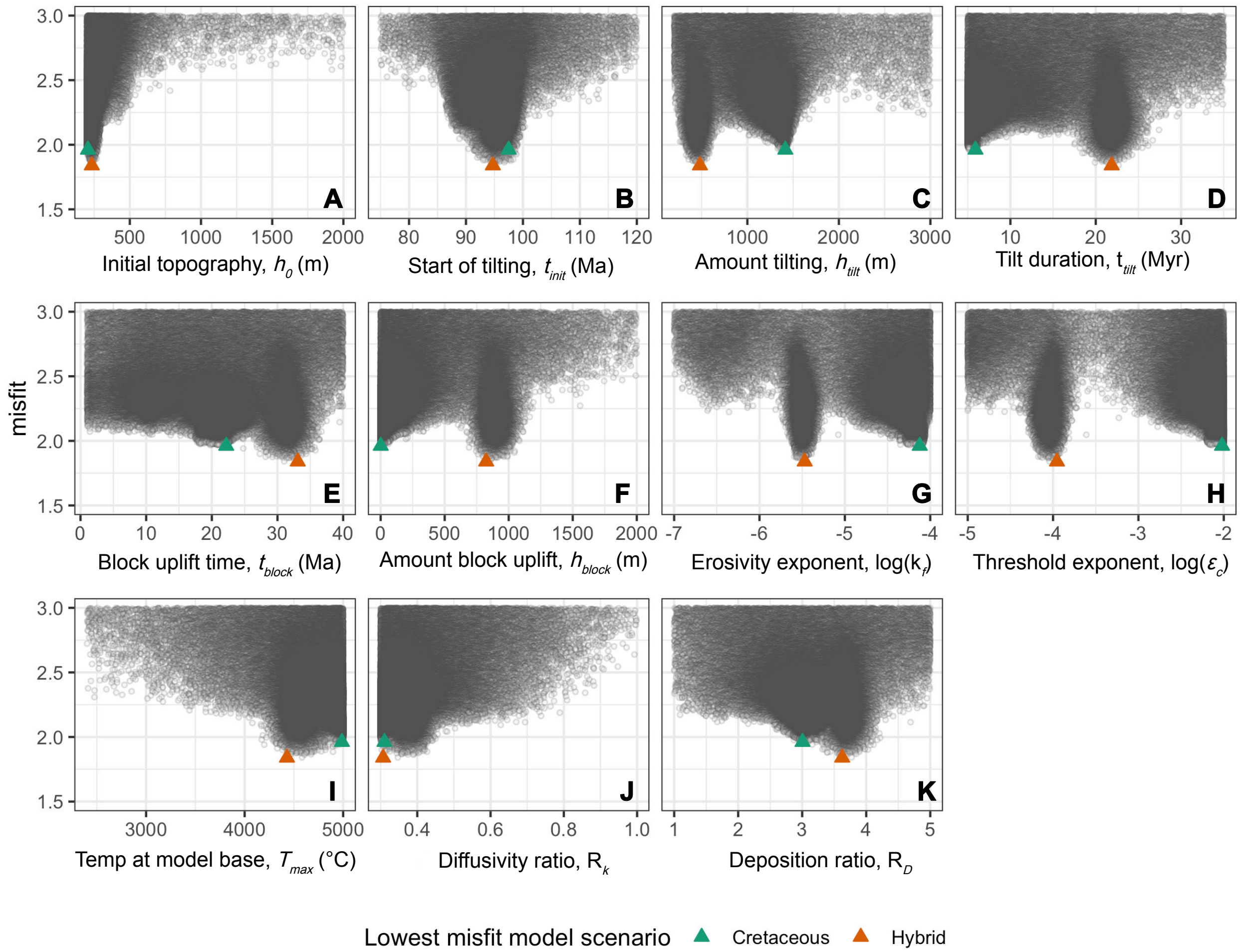

Figure 4: Plots showing the values of parameters for models with misfits < 3. Each grey circle represents one forward model and the value for a given parameter. The lowest points show the parameters converging toward value(s) with better fits to the data. Green and red-orange triangles show parameter values for best fit models from the Cretaceous and Hybrid Scenarios.

4. Results

4.1 Inversion Results

Results from topographic uplift driven inversions converge on two low-misfit parameter sets (Figure 4). Misfit values for individual forward model runs in the inversion range from 1.8 to >500, and these two clusters of low misfit solutions contain all of the model runs with misfit values less than 2. All low misfit models have similar thermal parameter values, with temperatures at the base of the 120 km thick lithosphere converging at >4000°C (Fig 4I), suggesting static geothermal gradients of >33°C/km, with the Karoo basin layer acting as a thermal blanket that is 2 to 3 times more insulating than the underlying basement (Fig 4J) leading to an even higher geotherm in the top 2 km. Finally, all models converge towards a value of 0.25 to 0.3 for R_D which indicates that only 1/3 to 1/4 of the volume of material eroded off the surface is deposited in the basin (Fig 4K).

The two parameter sets differ in the timing and magnitude of topographic uplift. Both indicate low initial topographies with plateau elevations <500 m (Fig 4A). Also, all low misfit models have some Cretaceous uplift initiating in the east between 100 and 90 Ma (Fig 4B). The two families of low misfit models differ in the magnitude of Cretaceous and Cenozoic uplift (Fig 4C, 4D, 4E, 4F). Figure 5 shows the topographic uplift over time for all models run, colored by misfit value. The lowest misfit models (yellow) clearly split into two uplift patterns. One group, which we will refer to as the Cretaceous Scenario, has ~1400 m of uplift in the Cretaceous, with dynamic tilting starting in the east, followed by uplift in the west that flattens the plateau after <10 Myr of tilting. This Cretaceous Scenario has very low magnitudes of uplift in the second Cenozoic block uplift phase, less than a few hundred meters, and the timing is not well constrained. The other group of low misfit models we will refer to as the Hybrid Scenario. These models have lower magnitudes of uplift during Cretaceous tilting, ~300-800 m initiating in the east at a similar time as the Cretaceous Scenario, but remain tilted for longer, >20 Myr, so uplift in the west occurs later (Fig 5). In the Hybrid Scenario, the majority of uplift occurs at ~35-25 Ma with > 800 m of Cenozoic block uplift. Both scenarios end with similar magnitudes of total uplift throughout the model run, on the order of 1500-1800 m, leading to a clear tradeoff between the amount of uplift in the Cenozoic and Cretaceous phases that is visible in a scatter plot of these parameter values and misfits (Fig 6A). Snapshots of the topography through time for the best fit models are shown in Figure 7 (also available as Movie S1 in the supporting information).

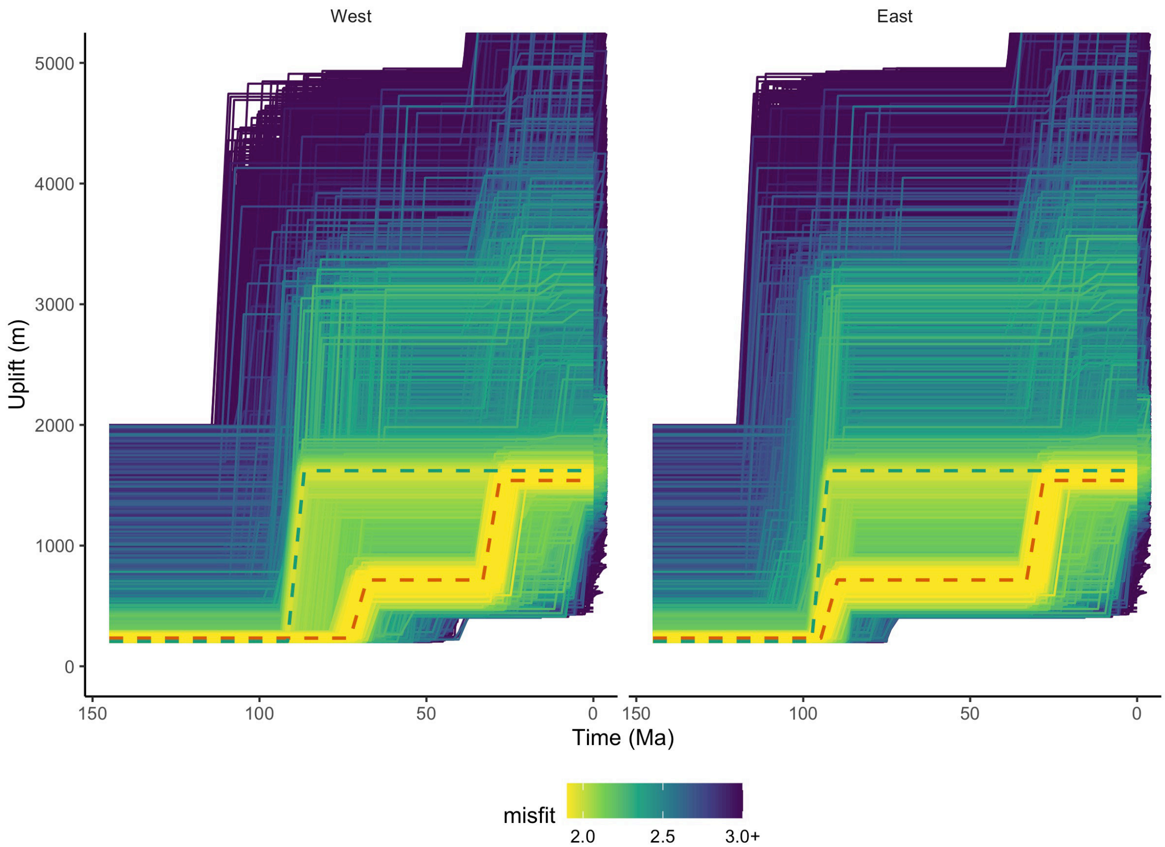

543 Figure 5. Uplift through time for the east edge (left panel) and west edge (right panel) of the model domain. Time is geologic time. Each line represents one forward model and is colored by the misfit value. Green dashed line is the best fit model for the Cretaceous Scenario and red-orange dashed line is the best fit model for the Hybrid Scenario.

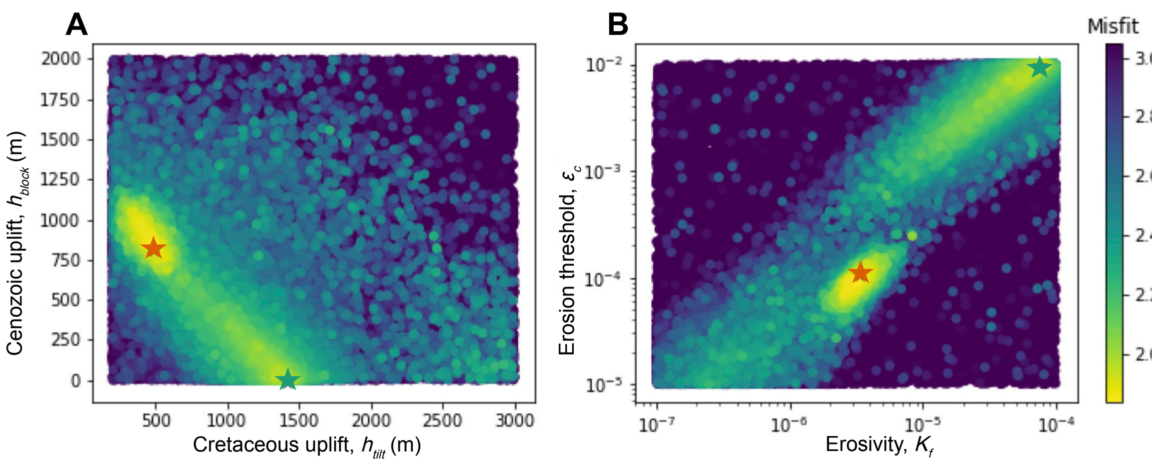

544 Figure 6. Scatter plots showing tradeoffs between parameter pairs. Each dot represents the parameter values for one forward model run and is colored by the misfit for the model. The low-misfit models show a tradeoff between the amount of Cenozoic uplift and the amount of Cretaceous uplift (A) as well as the erosion threshold and the erosivity (B). Green star shows the best fit model for the Cretaceous Scenario and red-orange star for the Hybrid Scenario. Many other combinations of model parameters are possible, but these two pairs show the strongest cross correlation.

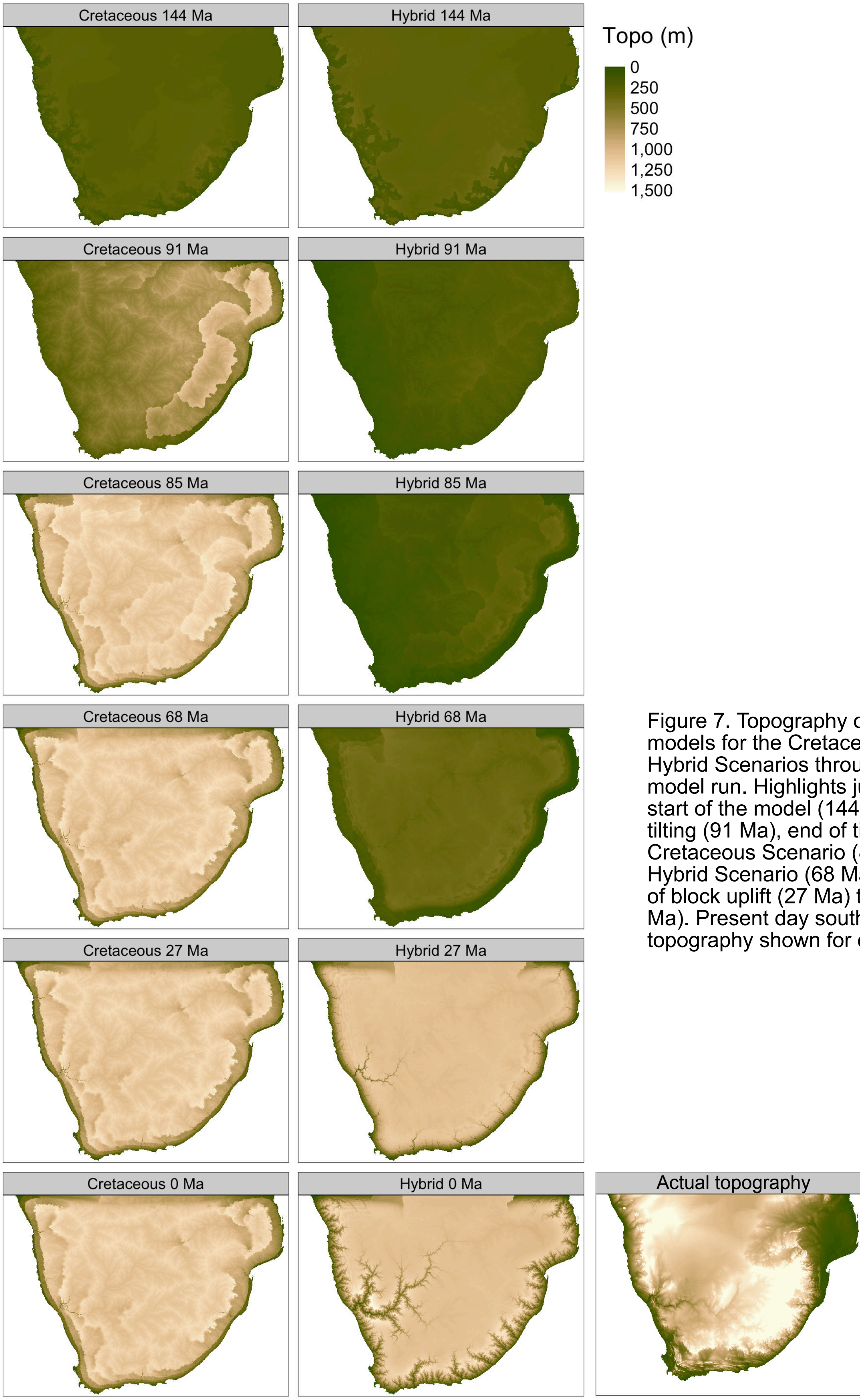

Figure 7. Topography of best fit models for the Cretaceous and Hybrid Scenarios through the model run. Highlights just after the start of the model (144 Ma), during tilting (91 Ma), end of tilting for Cretaceous Scenario (85 Ma) and Hybrid Scenario (68 Ma) and time of block uplift (27 Ma) to the end (0 Ma). Present day southern African topography shown for comparison.

545

The Cretaceous and Hybrid Scenarios differ most obviously in their uplift patterns, but they also converge to different erosional parameters (Figs. 4G, 4H). The Cretaceous Scenario converges towards values of the erosional parameter, K_f, between $2x10^{-4}$ and $6x10^{-4}$ $m^{0.2}$/yr and erosional threshold (ε_c) values of between $1x10^{-2}$ and $4x10^{-2}$ m/yr. The Hybrid Scenario converges with values for K_f and ε_c over an order of magnitude lower, with K_f between $4x10^{-5}$ and $9x10^{-5}$ $m^{0.2}$/yr and ε_c values of between $9x10^{-3}$ and $5x10^{-4}$ m/yr. This means that the Hybrid Scenario has relatively more durable material with K_f and a lower threshold for erosion as compared with the Cretaceous Scenario. There is also an tradeoff between K_f and ε_c that is visible in scatter plots of their parameter values and misfit (Fig 6B).

4.2 Data-Model comparison

The predictions from the lowest misfit model from the Cretaceous and Hybrid Scenarios are compared with the observed data in Figures 8 and 9. Overall the two models have a similar fit to the data. Both replicate the large pulse of sediment observed in the Orange River Basin in the Cretaceous and the overall lower fluxes observed elsewhere (Fig 8). Neither model produces the larger fluxes seen off the SW coast in the Cape Basin or in the Transkai Basin (Fig 8). Both models fit the median of the elevation, slope, and curvature distributions (Fig 9). Neither model produces the highest elevations, slopes, and curvatures observed in reality. The Hybrid Scenario has a closer match to the shape of the elevation distribution, while the Cretaceous Scenario fits the curvature distribution more directly. Neither model is able to reproduce the complexity observed in the thermochronology data, but both do a reasonably good job at replicating the average of the thermochronology dates, especially the AFT dates (Fig 9). The Cretaceous Scenario predicts overall slightly younger dates, which is a slightly better fit to the AHe dates especially. Overall, the models show fairly similar fits to the data and, while the models do not reproduce some of the details and structure in the natural data, they are a good match to the large-scale patterns observed.

5.Discussion

5.1 The role of data and the misfit function in identifying suitable models

A major and initially surprising take-away from the inversion results is that the existing data cannot differentiate between two low misfit parameter sets, at least with the data we

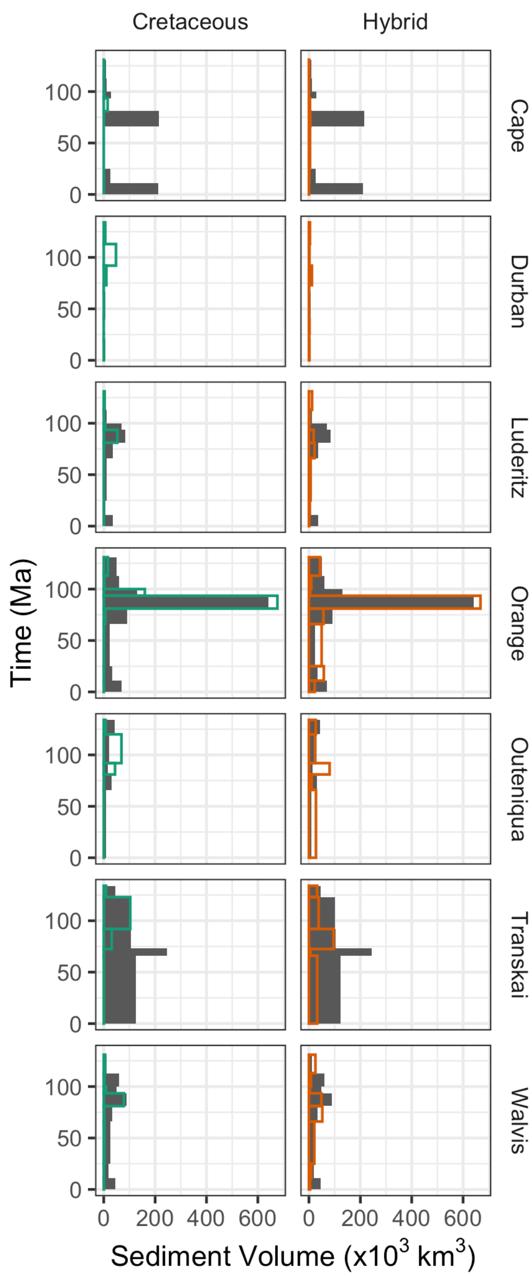

Figure 8. Sediment volumes through time from best fit models (colored outlines) compared with measured volumes from basins surrounding southern Africa (grey bars, Baby et al., 2020). See Fig 2 for locations of basins.

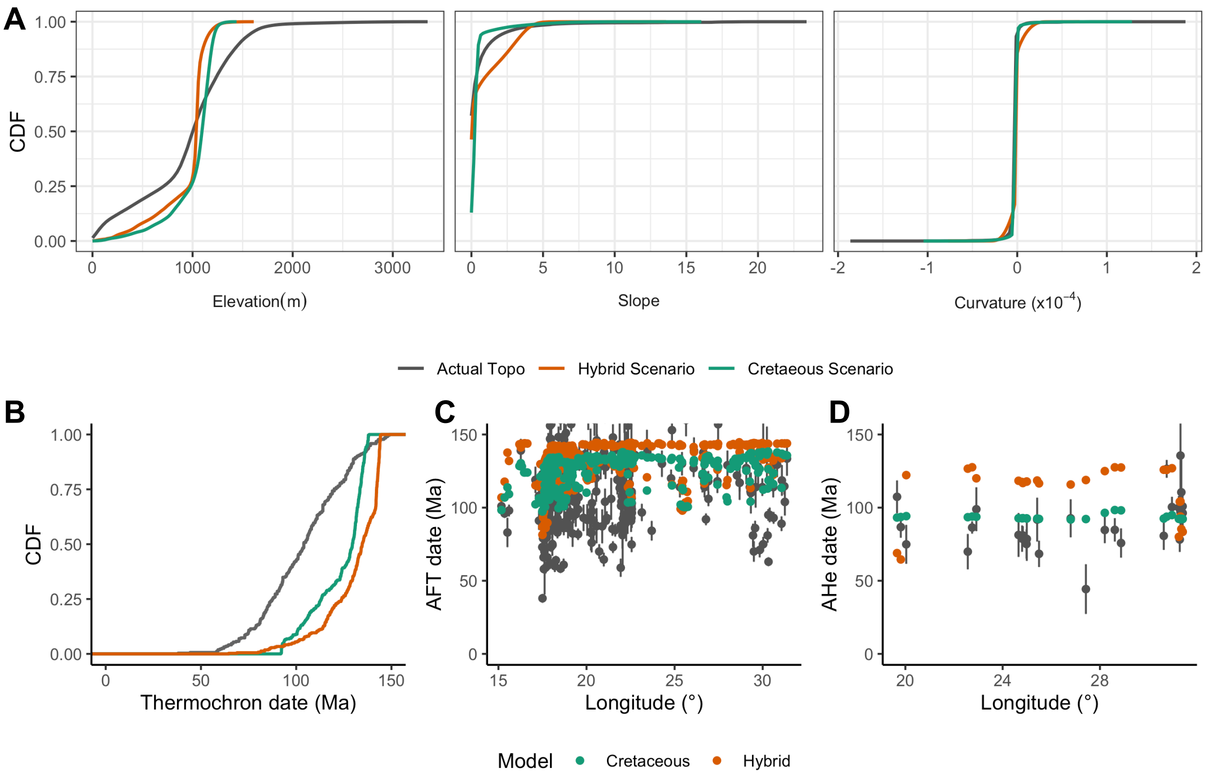

Figure 9. A) Comparison of CDFs of present day southern African topographic metrics (grey) to best fit model runs from the Cretaceous Scenario (green) and the Hybrid Scenario (red-orange). B) Comparison of the CDF for all thermochronology dates used in the inversion (AFT and AHe) between measured dates (grey) and modeled dates (colors). C) AFT dates plotted by longitude for observed data (grey) and modeled dates from the Cretaceous Scenario best fit (green) and Hybrid Scenario best fit (red-orange). D) same as in C but for AHe dates.

578

included and the current formulation of the misfit function. The uplift histories highlighted by the model inversions broadly match with times when plateau development had previously been proposed based on interpretation of the datasets that we have included (Table 1). We cannot settle the timing of uplift debate based on our results at present, but we can provide some insight into what is controlling the inversion results and what might allow future efforts to provide a more definitive answer.

The results of the model run are highly sensitive to the data used, the uncertainties associated, as well as the formulation of the misfit function and how those uncertainties are incorporated into the misfit function. No model is able to reproduce the observed data perfectly, and, given the simplifications made in the modelling exercise, we would not expect any model to truly be able to reproduce the complexities in the data. However, we constructed the misfit function to measure how well the model is able to capture the large scale trends in the data that we see as most important: the major pulse of erosion and sedimentation observed in the Cretaceous, low sedimentation and erosion rates observed in the Cenozoic, and plateau-like topography with similar statistical characteristics to the current topography. We made choices in constructing a misfit function that reflect our view of these as important aspects of the data. However, different formulations of a misfit function are possible and would strongly affect the inversion results. For example, there are many techniques that have been proposed for comparing model outputs to topography (e.g., Barnhart et al., 2020; Howard & Tierney, 2012; Ibbitt et al., 1999; Skinner et al., 2018) that range from direct pixel comparisons which retain the spatial information to wholly aggregated statistical comparisons. We have chosen to compare statistical distributions using the KS statistic because this is an appropriate measure of the broad similarities between the topographies, but if it was decided that specific topographic features were key to reproduce, a different metric might be more appropriate and it could change the outcome of the inversion.

Similarly, combining the metrics from different data types requires some challenging decisions about whether and how to weight the different data types that can potentially influence the inversion outcome. We have chosen not to weight the different misfits, and just sum them as the simplest solution. However, because the flux and thermochronology misfits take the form of least-squares differences and can range from 0 to large, while to topographic misfits can only range from 0 to 1, the combined misfit is more sensitive to the thermochronology and flux misfits even though we do not directly weight them. We feel that this is appropriate and that our inversion yields model results that fit all data types adequately compared with the several other misfit formulations that we tested. However, it should be noted that other choices about weighting of the different data types could be made, and these choices could substantially affect the inversion results.

Finally, the data included for comparison with model results strongly affects the inversion, and the inclusion of additional data has the potential to differentiate between these model scenarios. In fact, the results presented here can be used to guide future data collection efforts and highlight what additional information would be most useful in constraining the uplift histories of southern Africa. For example, the best fit models predict very different erosion rates in the final 1 Myr timestep (Figure 10), with the Hybrid Scenario predicting higher erosion rates focused along the main river network in canyons while the Cretaceous Scenario predicts very low erosion rates throughout the landscape. Cosmogenic radionuclide-based bedrock erosion rates can be compared to these predictions or included in future modelling efforts. Published cosmogenic radionuclide based erosion rates for southern Africa are mostly low (on the order of 10-6 m/Myr, Fig 10; Cockburn et al., 2000; Decker et al., 2013; Dirks et al., 2016; Erlanger et al., 2012; Fleming et al., 1999; Kounov et al., 2007; Makhubela et al., 2019; Scharf et al., 2013) but are generally not from within major river canyons, making it difficult to compare where the two landscape models differ the most prominently. One study focused directly on river valleys fairly high in the river systems near the drainage divide yields rates an order of magnitude higher, indicating there might be some spatial variation (Keen-Zebert et al., 2016). However, terraces in the lower Orange River suggest a maximum incision rate of 6 m/Ma post-17 Ma (M. C. J. de Wit, 1999). Additional data is needed to differentiate the two landscape models, and and the predicted patterns for recent erosion can provide guidance for future sampling campaigns.

Other aspects that future modelling could include are more complete of stratigraphic architecture rather than just sediment volumes, which might favor a post-Eocene phase of uplift (Baby et al., 2020; Baby, Guillocheau, Boulogne, et al., 2018; Baby, Guillocheau, Morin, et al., 2018). If future efforts were able to more precisely date the erosion surfaces and pediments, for example by (U-Th)/He dating of goethite, these could be more directly incorporated. A more nuanced, spatial comparison of the modelled and observed topography might capture some of the more distinctive features of southern Africa, potentially helping to distinguish uplift histories.

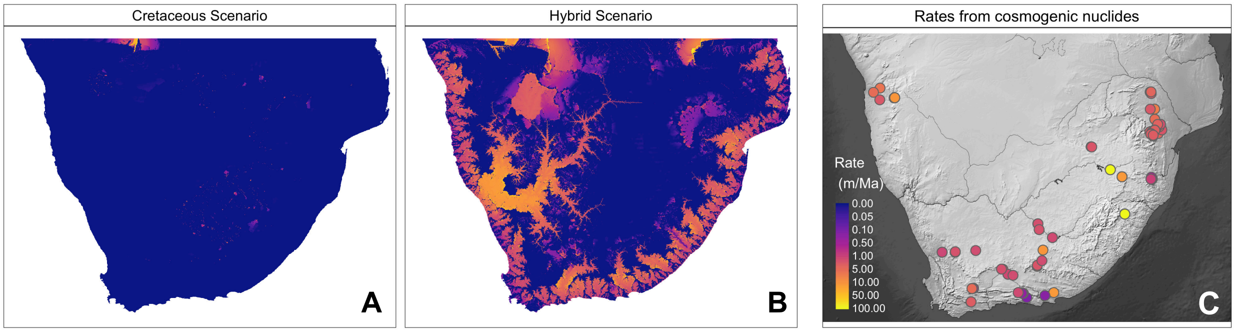

Figure 10. Predicted erosion rates for last 1 Myr timestep from each model (A, B) compared with recent erosion rates (over the last 0.1-2 Myr) derived from cosmogenic radionuclide studies (C). Data in C are published data from bedrock samples or river incision rates at particular locations (Kounov et al., 2007; 2015; Dirks et al., 2010; Cockburn et al., 2000; Erlanger et al., 2012; Glotzbach et al., 2016; Keen-Zebert et al., 2016; Bierman et al., 2014; Scharf et al., 2013; Decker et al., 2013)

641

5.2 Controls on erosional response to uplift

One of the challenges in elucidating paleotopography is how to quantitatively link erosion rates or magnitudes derived from the rock record to changes in surface uplift or topography. We make the assertion that we expect an erosional response to topographic uplift, but the question is how much uplift is required to trigger erosion of a given magnitude, and what might cause that to vary. By comparing to both topographic and erosional metrics in our inversions, the results give us some insights into which parameters are most strongly controlling the magnitude of erosion in response to the uplift we impose in the model, and what that might mean for southern Africa's uplift history. We find that in this case, the ratio between the erosivity coefficient, K_f, and our parameterization of an erosion threshold ε_c, plays an important role in the magnitude and temporal span of erosion after an uplift event. We also find that the shape of the uplift (tilting or block uplift) strongly effects the magnitude of erosion.

Braun et al. (2014) had already shown that continental tilting combined with a soft Karoo layer overlying harder basement was key for producing a sediment pulse similar to the major Cretaceous pulse in the Orange River Basin. Our results support that tilting is important and able to produce a large erosion response by steepening the slopes across the interior of the continent. Other shapes of uplift that we tried either disrupted the large, west draining Orange River drainage network, did not reproduce the sediment pulse, or both. In addition to the tilting, we found that adding a parameter representing a threshold for erosion was critical for reproducing the pulse as well as the low sedimentation rates observed on the southern coast and throughout the Cenozoic. Without this threshold, models would continue to erode substantially, especially around the plateau margins even after the continent was no longer tilted. There is a clear covariation between the threshold parameter, ε_c, and the erosivity, K_f, (Fig 6B) and parameter sets outside this band were not able to create the observed sediment pulse.

The Cretaceous uplift phase in both low misfit scenarios is able to produce similar magnitudes of erosion and sedimentation with very different magnitudes of uplift (Fig 11). The parameters controlling the magnitude of erosion in response to a given uplift magnitude are K_f and its ratio to ε_c, as well as the length of time the continent stays tilted. The Cretaceous Scenario has higher magnitudes of uplift and tilting, ~ 1400 m, but for a shorter total time, on the order of 5 Myr. It also has a higher base erosivity, but also a relatively higher threshold ($\varepsilon_c/K_f = 126$). Higher magnitudes of uplift and tilting are needed for stream power to exceed the threshold, but

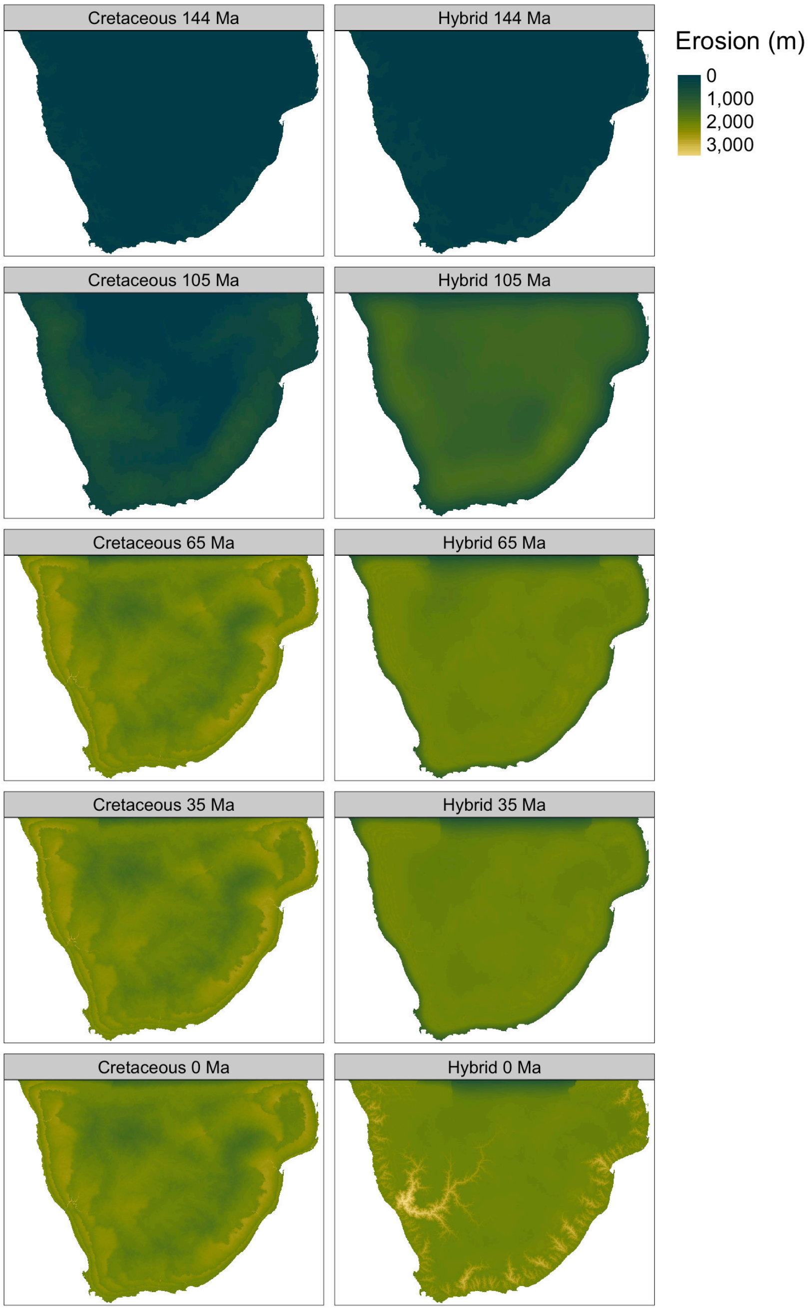

Figure 11. Erosion of the best fit models for the Cretaceous and Hybrid Scenarios throughout the model run. Highlights just after the start of the model (144 Ma), prior to Cretaceous tilting (105 Ma), after Cretaceous tilting (65 Ma), prior to Cenozoic block uplift (35 Ma) and after Cenozoic uplift at the end of the model run (0 Ma).

673

once exceeded, higher erosivity and steep slopes allow the model to erode relatively quickly. The Hybrid Scenario, which only has ~500 m of uplift during Cretaceous tilting, has a lower erosivity, but also a lower threshold with $\varepsilon_c/K_f = 33$ for the best fit model. It also remains tilted for longer, on the order of 20 Myr. This lower magnitude of tilt steepens slopes enough for stream power to exceed the threshold, and the continent remains tilted long enough for significant erosion to take place (Fig 11). The range in uplift magnitudes able to produce a similar erosion response highlights the difficulty in inferring uplift directly from erosion records, but also highlights the utility of landscape models, even fairly simple ones, to explore the range of possibilities.

The low magnitude erosional response to widely varying Cenozoic uplift in the two models further highlights the importance of the shape and style of uplift for how much erosion occurs. One of the longstanding debates about southern African topography is how much of the topography is "recent" which we define here as Cenozoic. The debate centers on two groups of apparently contradictory observations: geometric and geomorphic evidence supporting recent uplift, and extremely limited post-Cretaceous sedimentation and erosion arguing against a major recent uplift event. Historically, most of the evidence for recent uplift was based on geomorphic landforms that lacked quantitative dating (e.g., King, 1962 Partridge and Maud 1987), though more recent work inverting river profile shapes also suggests recent uplift (Paul et al., 2014; G. G. Roberts & White, 2010; Rudge et al., 2015). Terraces on the lower Orange River suggest 80-100 m of post-Miocene incision, while upstream and the Vaal-Orange confluence they suggest 120-140 m of incision (M. C. J. de Wit, 1999). Shoreline geometries contained in offshore stratigraphic architecture suggest continental uplift on the order of a few hundred meters at ~25 Ma on the east coast (Baby, Guillocheau, Boulogne, et al., 2018; Baby, Guillocheau, Morin, et al., 2018), and Pliocene marine terraces have been uplifted to ~400 m above sea level near Port Elizabeth (McMillan, 1990). In contrast, magnitudes of erosion since the Cretaceous are negligible in some locations by the preservation of crater facies kimberlites (Scholtz, 1985; Smith, 1986), and limited to less than 1-4 km by extensive low temperature thermochronology (Brown et al., 2002, 2014; Flowers & Schoene, 2010; Gallagher & Brown, 1999a; Kounov et al., 2009, 2013; Raab et al., 2005; Stanley et al., 2013, 2015; Stanley & Flowers, 2020; Tinker et al., 2008b; Wildman et al., 2015, 2016, 2017). Quantitative evidence on erosion has shown that erosion rates over the last ~2 Ma were slow based on cosmogenic nuclides (Bierman et al., 2014;

Chadwick et al., 2013; Decker et al., 2013; Dirks et al., 2016; Fleming et al., 1999; Kounov et al., 2007). There is very limited offshore sedimentation in the Cenozoic, also suggesting low erosion magnitudes on the continents (Baby et al., 2020; Baby, Guillocheau, Boulogne, et al., 2018; Baby, Guillocheau, Morin, et al., 2018; Guillocheau et al., 2012; Rouby et al., 2009; Tinker et al., 2008a), and near Cape Town, essentially no incision since the Miocene (D. L. Roberts et al., 2013). Together this suggests either limited recent surface uplift or that almost no erosion was caused by any recent uplift.

One way to reconcile these seemingly contrasting observations (geometric evidence for recent uplift but very low erosion rates) is if surface uplift does not trigger a large erosional response. The Hybrid Scenario model demonstrates that limited erosion in response to substantial surface uplift is possible from a geomorphic standpoint. Normally, surface uplift is thought to trigger an erosional response by steepening slopes and increasing stream power and therefore erosion rates. In the case of the Hybrid Scenario, block uplift of an already low-relief plateau only causes steepening in very focused locations in river channels. Therefore, even though substantial topography is developed in the Cenozoic in the Hybrid Scenario, the erosional response is subdued across most of the landscape, reconciling the low eroded volumes and generally low erosion rates with geometric evidence for surface uplift.

5.3 Source-to-sink mass balance

The interest in topographic evolution, confined marine basins, and limited to absent continental sediment storage in southern Africa make it an advantageous location to study source to sink relationships. The extensive data coverage and the use of the landscape model to directly calculate denudation magnitudes and thermochronology dates with an evolving crustal thermal structure allows us to examine the source-to-sink mass balance more holistically than previously possible. Past work compared estimated onshore denudation through time from AFT data to marine sediment volumes on the west coast and the south coast with differing results. Rouby et al. (2009) compared the marine sediment volumes from the west coast basins to AFT derived denudation magnitudes for the western margin of southern Africa and Namibia (Gallagher and Brown, 1999a, 1999b) and found a reasonably good match of the volumes through time with the exception of the Cenozoic. On the southern margin, Tinker et al. (2008a, 2008b) compared the AFT derived denudation and sediment volume in the Outeniqua Basin and found that the marine sediment volumes were an order of magnitude less than onshore denudation volumes, though the patterns timing of denudation and deposition match well (Tinker et al., 2008a). The marine sediment volumes calculated by Tinker et al. (2008a) where based on only the shelf volumes, so any material deposited in the deep sea was unaccounted for (Baby et al., 2020; Tinker et al., 2008a). Richardson et al. (2017) estimated the eroded volume on the south coast using geometric reconstruction of onshore sedimentary units and suggested that only one third to one half of the eroded volume was contained in the Outeniqua Basin.

Our model provides a new way to examine this question by searching for erosion histories that can match both the thermochronology data and the offshore sediment volumes. There are several key parameters used to calculate thermochronology dates from erosion histories, and by examining the ranges of these parameters that are able to satisfy both the thermochronology and the sediment data we can gain insights into source to sink relationships. Thermochronology is highly sensitive to the upper crustal thermal structure, and previous thermochronology based denudation estimates (Gallagher & Brown, 1999a, 1999b; Tinker et al., 2008b; Wildman et al., 2015, 2016) made some set of assumptions for this structure through time, which could be a source of uncertainty when comparing onshore denudation and offshore volumes. We calculate the thermal structure throughout the model run, and key parameters controlling the structure are the temperature at the base of the model (T_{max}), the ratio between the thermal diffusivity of the basement and the overlying Karoo sedimentary rocks (R_K). We vary both T_{max} and R_K, as well as adding an additional non-thermal parameter which represents the ratio of sediment volume lost between onshore erosion and offshore deposition (R_D). T_{max} can range from 2400 to 5000°C (Table 2) which represents static geothermal gradients of 20-42°C/km given the 120 km thick model, and R_K varies from 0.3 to 1 ranging from substantial thermal blanketing by the Karoo sediments to no effect. Low misfit models converge with thermal parameters suggesting higher static geothermal gradients (>34°C/km) and more extreme thermal diffusivity ratios, where thermal diffusivity is 50% or less in the Karoo sediments as compared with the basement (Fig. 4I, 4J). The combination of higher temperatures and the base of the model and high thermal blanketing means that the low misfit models have higher geothermal gradients in the upper crust, therefore requiring lower magnitudes of exhumation to produce the observed thermochronology dates. Even with these values for the thermal parameters, low misfit models converge on values of the deposition ration, R_D, where only ½ to ¼ of the eroded material is deposited in the basins (Fig 4K).

There are several caveats to this ratio, however. The first is that there are tradeoffs between all of these parameters. More extreme geothermal gradients or thermal diffusivity ratios (outside the range over which parameters were allowed to vary) would require less denudation to satisfy the thermochronology data, yielding a lower mismatch between the predicted and observed volumes. Additionally, while the predicted sediment volumes match the observed sediment volumes well for certain times throughout the model run, particularly in the Cretaceous, there are other times when the model predictions underestimate the volume of sediment (Figure 7). Since at times the model underestimates the sediment volume, the ratio of sediment loss implied by the parameter R_D in the low misfit models is likely an upper limit for sediment loss. Also, in reality the ratio of sediment loss may have been variable through time while R_D is fixed throughout a model run. Despite these caveats, the models suggest that more material is eroded than deposited in the marine basins, perhaps greater than twice as much.

This, of course, begs the question of what happened to this "missing" sediment? We see three possible explanations: 1) material was removed from the system via tectonic transport out of the region, 2) material was removed from the system via oceanic transport out of the area, or 3) material was removed from the continent via chemical denudation and therefore not deposited as a solid load in the basins. We favor this as evidence of substantial chemical denudation on the continent, but we will examine the evidence for each of these mechanisms.

There is clear evidence that some material eroded off the southern coast during the early portion of Gondwana breakup was deposited in the marine basins that are presently near the Falkland Plateau, now situated in the SW Atlantic Ocean. In the Late Jurassic and Early Cretaceous this basin was situated adjacent to the Outeniqua Basin (Baby, Guillocheau, Boulogne, et al., 2018; R. V. Dingle & Scrutton, 1974; Macdonald et al., 2003; Martin et al., 1982; Richardson et al., 2017; Williams, 2015). The North Falkland Basin contains continental facies, likely derived from southern Africa (Baby, Guillocheau, Boulogne, et al., 2018; Richardson et al., 2017; Williams, 2015). The main period of southern African deposition into this basin was ~135-130 Ma, after which transform motion on the Agulhas-Falkland Fracture Zone and eventual opening of the South Atlantic removed the North Falkland Basin from proximity to southern Africa (Baby, Guillocheau, Boulogne, et al., 2018; R. V. Dingle &

Scrutton, 1974; Martin et al., 1982). Thus any sediment loss due to tectonic transport is limited to the Early Cretaceous.

Several erosional features and contourites deposits present on all margins show that sediments have been eroded and redistributed since the Lower Cretaceous by oceanic processes (e.g., Baby, Guillocheau, Boulogne, et al., 2018; Hopkins, 2006; Thiéblemont et al., 2020; Uenzelmann-Neben et al., 2007). Oceanic current structures have been characterized at various depth since Aptian - Albian times (120-110 Ma) in Walvis and Zambezi Basins, but their role became major during Early Miocene (23-16 Ma, Hopkins, 2006; Thiéblemont et al., 2020; Uenzelmann-Neben et al., 2007). The ability of these oceanic currents to transport large volumes of sediment (here during Neogene times) is difficult to quantify, even though it is of primary importance in modeling source-to-sink systems. Concerning surficial currents, Orange River sand is known to be transported up 1000+ km northward up the Namibian coast via littoral drift (e.g., Garzanti et al., 2018) but the amount of sand transported is estimated at 1500-15000 km^3 over the last 15 Myr (Garzanti et al., 2018) which only amounts to a small fraction of the west coast sediment budget. In summary, the magnitude of sediment lost due to oceanic transport is unknown. It may be significant, particularly in the Miocene, but sediment lost this way varies in space and time.

Finally, chemical weathering on the continent could have been substantial. Basalts are particularly susceptible to chemical weathering (e.g., Dessert et al., 2003; Dupré et al., 2003) and much of the eroded material in the Cretaceous was Karoo flood basalts (e.g., Hanson et al., 2009; Stanley et al., 2015; Tinker et al., 2008a). To add to that, Cretaceous erosion took place under climatic conditions much warmer than today, which could have promoted chemical weathering (e.g., Cohen et al., 2004; Jenkyns et al., 2004). A rough compilation of precipitation records based on paleobotanical data suggests a sharp change around 85 Ma from semi-arid to very humid conditions favoring intense silica weathering up to 40 Ma (Braun et al. 2014). Deep weathering surfaces are found throughout southern Africa (e.g., Summerfield, 1983). North of our study area, such weathering surfaces were dated in southern Congo (Katanga) based on supergene manganese ore between to 77 Ma and 2 Ma with several peaks, demonstrating many phases of weathering and surface formation since the Cretaceous (De Putter & Ruffet, 2020). Within our study area there is evidence for the role of chemical weathering in the denudation history in some locations (e.g., Chadwick et al., 2013; Margirier et al., 2019).

Overall, our model results suggest that a substantial volume of material eroded from the continent was not accounted for in the sediment volumes presently in the marine basins. This sediment loss was likely due to a combination of factors, and the most important process may have varied through time. In the Early Cretaceous, sediment could have been deposited on the Falkland Plateau (e.g., Baby, Guillocheau, Boulogne, et al., 2018; R. V. Dingle & Scrutton, 1974; Martin et al., 1982), while oceanic currents may have redistributed substantial volumes especially in the Neogene (e.g., Thiéblemont et al., 2020; Uenzelmann-Neben et al., 2007) (e.g., Uenzelmann-Neben et al., 2017; Thiéblemont et al., 2020). Throughout the history, but especially during the Late Cretaceous and Paleogene, substantial denudation may have occurred via chemical processes resulting in less sediment deposited as a solid load in the basins. Our best fitting models match the observed sediment volumes best in the Late Cretaceous (Fig 8) with only ~1/3 of the eroded sediment being deposited in the basin. Climatic conditions were favorable for chemical weathering at that time (e.g., Braun et al., 2014) and we take our results to provide support for substantial continental chemical weathering in southern Africa, especially in the Late Cretaceous and Paleogene.

5.4 Climate?

A weakness of our modelling approach is that we do not consider the role of climate or precipitation changes through time. It is beyond the scope of this particular study to explore those effects in full, but as a test to understand the magnitude of potential effects we ran an additional inversion where we varied precipitation instead of uplift parameters. The goal of this exercise was to test whether variations in precipitation alone could explain the observations. In these models, initial topography was allowed to vary between 0 and 2000 m and then no other uplift besides the isostatic response to erosion was imposed. This essentially is prescribing that plateau uplift pre-dates the start of the model at 145 Ma. Precipitation rate was allowed to increase by a factor of 0 to 100 for a period of 5 to 40 Myr in the Cretaceous, before returning to the background rate, with an option of varying again by another factor from 0 to 100 in more recent times (Table S3, Figure S1). This mirrors the structure of the uplift scenarios, but instead varies precipitation rate (Figure 12, Table S3, Figure S1). In addition to precipitation rate, we also allowed the erosional and thermal parameters varied in the uplift scenarios to vary.

This inversion converges on a parameter set that is able to reproduce the observations with misfits <2, a similar level to the two best-fitting scenarios for the uplift driven cases. Some parameters are more tightly confined than others, but the lowest misfit models have ~1400 m of initial topography, an increase in rainfall of >50 times the base rainfall starting at ~95 Ma and lasting for 20 to 40 Myr before returning to the background value (Fig 12). This is followed by a second uptick in precipitation by again >50 times background in the last 35 Myr. This suggests that precipitation changes could potentially play an important role in the erosion history, but we should first examine how realistic these results are.

Assuming a reference present-day rate of precipitation of 0.8 m/yr, an increase by a factor of 50-100 would mean that the low misfit models require 40-80 m/yr of precipitation in the Cretaceous. Maximum annual rainfall at present, globally, is on the order of 10 m/yr, so these values seem unrealistically high, though the Cretaceous had a substantially different climate than today. Global reconstructions suggest that climate in southern Africa was arid in the early to mid-Cretaceous, moving toward humid starting at ~85 Ma to the end of the Cretaceous (Chumakov et al., 1995; Hay & Floegel, 2012). Continental paleoprecipitation records derived from southern Africa during the Cretaceous are unfortunately sparse, but fossil evidence from the Atlantic coastal margin indicates progressive drying from ~130 to 90 Ma and a change from arid or semi-arid conditions to humid at ~85 Ma (Bamford & Stevenson, 2002; Braun et al., 2014; Sandersen, 2007). On the Indian coastal margin this transition began earlier, ~90 Ma (Ponte et al., 2019). Limited evidence suggests humid conditions on the coastal plains until the beginning of the present arid period, which began on the Atlantic margin ~15 Ma (Braun et al., 2014; Pickford et al., 1999; Ponte et al., 2019; Senut et al., 2009). On the plateau surface fossil records are limited to a kimberlite pipes which preserve crater lake sediments. These suggest different conditions from the coastal plains with temperate to mildly humid conditions at ~95-90 Ma (Rayner et al., 1997) and dry temperate conditions at ~70-65 Ma (Smith, 1986).

Evidence for wetting of the climate on the coastal plains in the mid-Cretaceous could be consistent with the increase in precipitation rate required by the precipitation-driven models from 95-90 Ma. However, the observations suggest the climate transition on the Atlantic margin post-dates the timing of increased rainfall in the model by 5-10 Myr, and it appears there were different conditions on the plateau and the coastal plains. A 50x or more increase in rainfall across the entire plateau is somewhat difficult to reconcile with the observations. There is also no

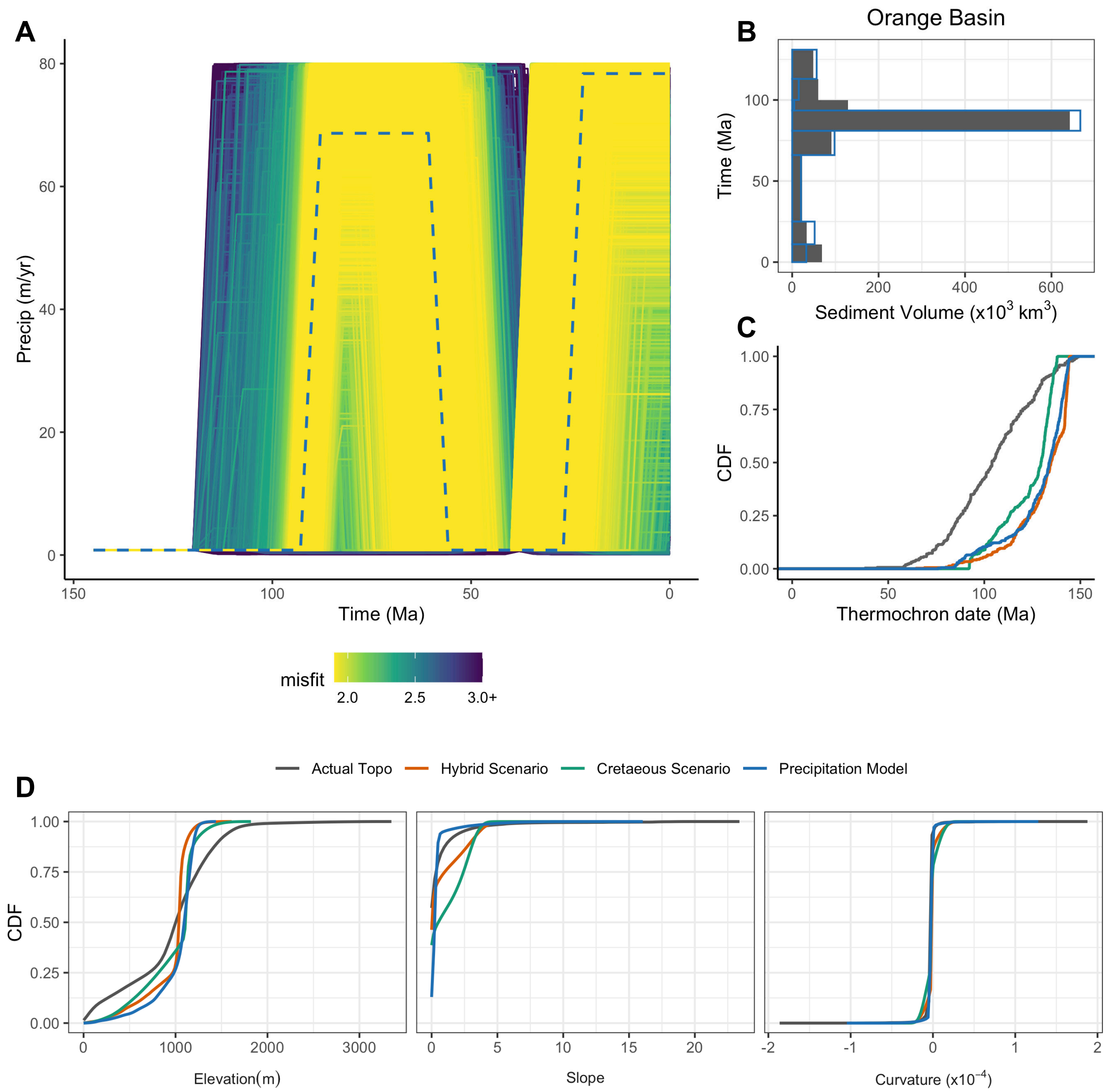

Figure 12. Results from precipitation variation inversion model. A) Paths showing precipitation magnitude over time for forward models, colored by misfit with yellow being good fits to the data. Blue dashed line shows best fit model. B) Comparison of the observed sedimentary flux in the Orange Basin (grey boxes) with predictions from the best fit precipitation-driven model (blue). C) Comparison of the CDFs for all published thermochronology dates (AFT and AHe, see Fig 2) with those predicted by all three best fit models - the Cretaceous Scenario (green), the Hybrid Scenario (red-orange), and the model driven only by precipitation (blue). D) Comparisons of the topographic metrics of the observed topography and all three best fit predictions.

obvious evidence for the marked decrease in rainfall in the models in the latest Cretaceous or early Cenozoic, and the high rainfall amounts predicted by the model since the mid-Cenozoic are also inconsistent with the dominantly semi-arid to arid conditions on most of the plateau today.

On the whole, while an extreme increase in rainfall can reproduce the observed Cretaceous erosion pulse, it is not realistic as the sole driver for this erosion event. We interpret these results to mean that while precipitation or climate changes likely played a role in southern Africa's erosion and topographic history, they cannot realistically explain the magnitude of erosion that is observed without any topographic uplift. This is in concert with geometric evidence for continental uplift from marine archives that cannot be caused by changes in climate alone (Baby et al., 2020; Baby, Guillocheau, Boulogne, et al., 2018). It is also worth noting that changes in topographic conditions could cause changes in local climate and precipitation conditions through orographic effects. For example, development of a plateau in the mid-Cretaceous could induce a transition to wetter conditions on the coastal plateau margins and maintain dryer conditions within the plateau interior, a scenario which is consistent with the fossil record.

5.5 Distinguishing geodynamic mechanisms for plateau uplift

Both the Cretaceous Scenario and the Hybrid Scenario predict some topographic development in the Cretaceous but the two scenarios differ in magnitude and the duration of continental tilting during this uplift phase. We can compare the rates and magnitudes from our models to those which might be expected from different geodynamic mechanisms for uplift. Both models predict a total of ~1400 m of dynamic topography by the end of the model run. This is within, but on the upper end, of the range of predicted magnitudes of present day dynamic topography in southern Africa, though it should be noted that these predictions vary widely (e.g., Flament et al., 2013). However, the two scenarios differ in the timing and rate of topographic development (Fig. 13). The Cretaceous Scenario has a much higher uplift magnitude during dynamic tilting than the Hybrid scenarios (1414 m vs 482 m for their respective best fit models, Fig. 13). We can also compare both vertical uplift rates and horizontal propagation rates. One of the fixed parameters in all models is that the dynamic uplift occurs linearly over 5 Myr. The Cretaceous Scenario then has a dynamic uplift rate of 0.28 mm/yr, while the Hybrid Scenario uplifts at a rate of 0.1 mm/yr. To approximate the horizontal propagation rates for the uplift

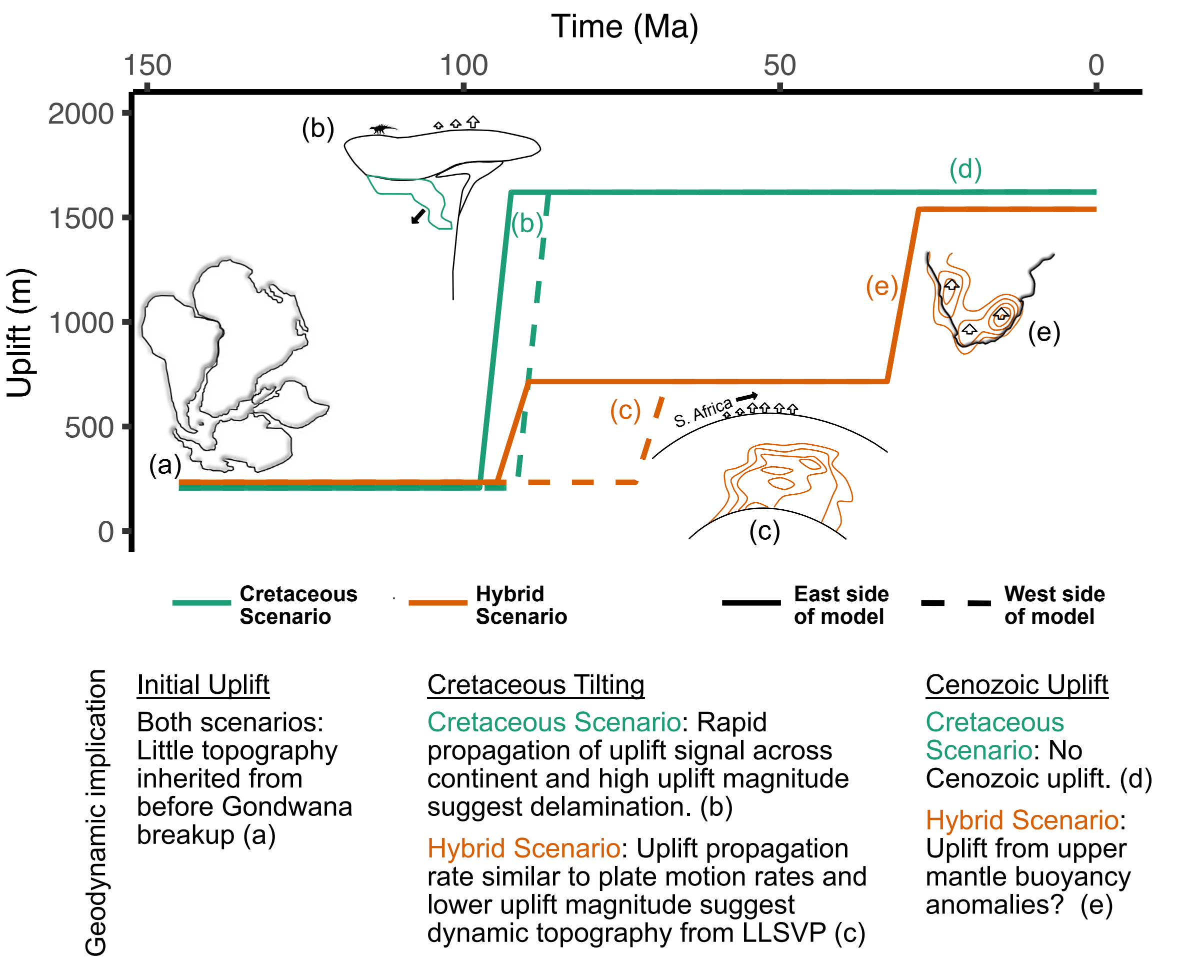

Figure 13. Geodynamic implications of the model results. Lines on graph show uplift over time for best fit models from the low misfit regions of model results. Cartoons show implied geodynamic mechanism for each uplift phase. See text for a more complete discussion and Table 1 for more on geodynamic hypotheses.

signal, we can use the tilt time parameter and the width of the model. The tilt time parameter is the time delay between the east side of the model initiating uplift and the west side (Fig. 13). In essence, it is the amount of time it takes the uplift to propagate across the model domain. A rough estimate of the horizontal propagation rate that can be compared to plausible geodynamic deformation rates is given by dividing the 2365 km wide model domain by the tilt time (5.9 Myr for the best fit Cretaceous Scenario and 21.7 Myr for the best fit Hybrid Scenario). The propagation rate of the uplift is then 40 cm/yr for the Cretaceous Scenario and 11 cm/yr in the Hybrid Scenario.

Braun et al. (2014) proposed that tilting and dynamic uplift of the plateau was caused by movement of the African plate over the LLSVP in the deep mantle. In this conceptual model, rates of horizontal propagation should be set by plate motion rates. Both the Cretaceous and Cenozoic propagation rates are fast for plate motion rates, but the Cretaceous Scenario especially so. Plate motion rates reconstructed for Africa in the mid-Cretaceous vary. Colli et al. (2014) reconstructed absolute plate speeds for a point in the northwest quadrant of our model (27°S, 15°E) using the Müller et al. (1993) fixed hotspot reference frame and a combination of the O'Neill et al. (2005) and Steinberger and Torsvik (2008) moving hotspot and true polar wander models. The fixed hotspot frame gave velocities increasing from <1 to ~3 cm/yr from 110 to 90 Ma (Colli et al., 2014; Müller et al., 1993), while the moving hotspot and true polar wander models gave velocities ranging from ~2 to 4 cm/yr between 110 and 90 Ma with a major spike to >10 cm/yr between 105 and 100 Ma (Colli et al., 2014; O'Neill et al., 2005; Steinberger & Torsvik, 2008). These rates are all substantially below the 40 cm/yr predicted by the Cretaceous Scenario but begin to approach those of the 11 cm/yr predicted by the Hybrid Scenario at times.

In addition to propagation rates that are too fast to be dictated by plate motion of southern Africa riding over the LLSVP, the Cretaceous Scenario requires a high magnitude of Cretaceous topography, ~1400 m. While initial work suggested that this magnitude of dynamic topography could be attributed to the LLSVP (e.g., Lithgow-Bertelloni & Silver, 1998), more recent studies suggest that the large degree-two lower mantle structures have a more limited influence on dynamic topography at the surface (Hoggard et al., 2016; Osei Tutu et al., 2018; Steinberger, 2016; Steinberger et al., 2019; Watkins & Conrad, 2018). Together, this implies that if the Cretaceous Scenario is the correct model, some other mechanism beyond dynamic topography over the LLSVP needs to be invoked to explain the rapidity and magnitude of elevation gain.

Removal of mantle lithosphere either through delamination or dripping of convective instabilities could potentially generate these magnitudes and rates. Hu et al. (2018) proposed a delamination-style peeling back of the lowermost lithosphere triggered by motion over hotspots, also implying that rates would dominantly be controlled by plate motion rates. However, at least for lithospheric drips, dynamic models show that once instabilities form, they can grow exponentially or even super exponentially depending on the wavelength of the perturbation and the viscosity structure (e.g., Conrad & Molnar, 1997; Molnar et al., 1998). So perhaps once destabilized the dense lower lithosphere could have been removed fairly rapidly. Dripping or delamination can also produce surface uplift on the order of 1-2 km (e.g., Göğüş & Pysklywec, 2008a, 2008b) in line with the uplift required by our Cretaceous Scenario. There is also evidence for Cretaceous lithospheric perturbation in southern Africa from elevated geothermal gradients recorded by mantle and lower crustal xenoliths (Bell et al., 2003; Schmitz & Bowring, 2003) and the coincidence of a major erosion phase with this warming geotherm (Stanley et al., 2013). If the Cretaceous Scenario is correct, we suggest much of the uplift of southern Africa was driven by lithospheric foundering rather than solely sublithospheric dynamic topography (Fig. 13).

The Hybrid Scenario has smaller magnitudes (400-500 m) of dynamic topography in the Cretaceous and propagation rates that are more consistent with plate motion reconstructions, followed by ~800 m of uplift in the Cenozoic. Retrodictions of dynamic topography back through the Cretaceous are somewhat limited, but several predict the development of 200-500 m of dynamic topography during the early Late Cretaceous, due to motion over the LLSVP and/or motion away from the South American subduction zone (Flament et al., 2014; Rubey et al., 2017; Zhang et al., 2012). Motion of southern Africa over the LLSVP and deep-mantle derived dynamic topography seems to provide a suitable explanation for the magnitudes and rates of Cretaceous topographic development in the Hybrid Scenario (Fig. 13). Interestingly, the peak in southern African plate motion rate in the moving hotspot/true polar wander reference frame (Colli et al., 2014; O'Neill et al., 2005; Steinberger & Torsvik, 2008) most closely corresponds with the rates in the Hybrid Scenario and also coincides with the initiation of Cretaceous uplift. Colli et al. (2014) argued that changes in South Atlantic spreading velocities are related to topographic changes on the continents through pressure driven flow in the asthenosphere. Together this highlights the potential links between the deep earth, plate motions, and continental erosion. An additional ~800 m of Cenozoic dynamic topography in the Hybrid Scenario onsets at

30-35 Ma. This also coincides with a rapid phase of south Atlantic spreading (Colli et al., 2014), as well as the proposed timing for development of small-scale convection beneath Africa (Burke, 1996), and overlaps with development of the East Africa Rift system (e.g., Ebinger & Sleep, 1998; E. M. Roberts et al., 2012). Development of this Cenozoic topography seems more likely to be derived from upper mantle density anomalies than the LLSVP, though both could contribute (Hoggard et al., 2016; Winterbourne et al., 2009).

The Hybrid and Cretaceous Scenarios have different magnitudes and rates of uplift, implying different driving mechanisms for uplift (Fig. 13). We do not strongly favor one over the other but note that an area for future work could be to compare our low misfit models directly with geodynamic models, particularly since the driver for dynamic topography in the landscape model is a basal stress.

6. Conclusions

We used inversion methods to compare landscape models varying a range of uplift, erosion, and thermal parameters with observed offshore sediment volumes, thermochronology data, and topography from Southern Africa. We explored three proposed hypotheses for when the plateau was elevated and found good matches to two possible uplift histories (Fig. 3) . One suitable model has plateau development entirely in the Cretaceous, with ~1400 m of dynamic uplift and continental tilting over ~6 Ma between 100 and 90 Ma. The other suitable model has two phase plateau development with ~500 m of dynamic uplift and continental tilting from ~100-75 Ma followed by ~800 m of dynamic block uplift at ~30 Ma (Fig. 5). The data that we used cannot distinguish between these two uplift histories, though stratigraphic architecture at the margins suggests two phases of uplift (Baby et al., 2020; Baby, Guillocheau, Boulogne, et al., 2018; Baby, Guillocheau, Morin, et al., 2018). However, model predictions can be used to identify data that could be used to differentiate between these model predictions. For example, the best fit models for each uplift history differ markedly in both the rates and patterns predicted for erosion rates over the last 1 Myr, and studies could be designed to target areas of expected differences using cosmogenic radionuclides (Fig. 10).

Results from these models give some insight into the link between erosion rate, uplift, and topography in southern Africa. Good fitting models show an important relationship between the magnitudes of the erosivity constant, K_f, and our parameterization of an erosion threshold, ε_c

(Fig. 6). This suggests that a fairly high threshold is important for maintaining uplifted topography over long periods of geologic time with low erosion and sedimentation rates. In addition to the erosive parameters, the erosional response to uplift is highly sensitive to the shape of the uplift. Our models show that continental scale tilting can cause a high magnitude erosional response for a range of uplift amounts due to steepening of the entire drainage network and stability or enhancement of large drainages. This is in line with previous work (Braun et al., 2013, 2014) and is important for reproducing the pulsed nature of Cretaceous erosion and sedimentation in southern Africa. In contrast, the block uplift shape produces a relatively small erosional response for significant magnitudes of uplift because much of the plateau interior does not steepen (Fig. 11). These conditions are able to reconcile geometric evidence for Cenozoic uplift with the observed low magnitudes of erosion.

Source to sink mass balance between the amount of material eroded implied by the thermochronology data and the amount deposited in the offshore basins suggests a substantial amount of mass loss. Best-fit models suggest about 3 times as much material was eroded as deposited. While some material could have been transported away by ocean currents or tectonics (Garzanti et al., 2018; Richardson et al., 2017), we argue that this is evidence for substantial chemical denudation, where a large portion of the material removed from the continent was transported in solution to the ocean and therefore not directly deposited in marine basins. This has potential implications for climate and the nature of cratonic erosion that could be explored further with future work.

We did not vary climate or precipitation in our models, but to test the extent to which this could affect the results we ran one additional inversion where no uplift was imposed on the model, but precipitation magnitude was allowed to vary through time. We found some precipitation-only models were able to match the observed data as well as the uplift driven models, but only if average precipitation ranged over two orders of magnitude up to unrealistically high amounts (Fig. 12). Precipitation variability could have played an important role in southern Africa's erosion history, but it cannot realistically explain the observations without topographic uplift. The relative roles of these processes in southern Africa merits more exploration in the future.

Finally, while the data cannot distinguish between the Cretaceous and Cenozoic best fit models at the present, the relative rates of deformation and magnitudes of surface change might help discriminate between the geodynamic mechanisms which could be driving them (Fig. 13). For the Cretaceous Scenario, the propagation of the uplift signal during continental tilting is likely too rapid to be only related to plate tectonic motion, and uplift magnitudes are higher than expected for dynamic uplift due to the LLSVP. Uplift in this case may be more likely to be driven by processes that can act faster and cause more surface change like delamination (e.g., Göğüş & Pysklywec, 2008b; Hu et al., 2018) than by the African Plate moving over the LLSVP (Braun et al., 2014). However, in the Hybrid Scenario uplift propagates across the continent at a rate more in line with plate motions, and uplift magnitudes are lower. Thus, tilting as the African Plate rides over the LLSVP is a highly plausible uplift mechanism. Geodynamic models could be directly compared to, or even constrained by the results presented here.

Acknowledgments, Samples, and Data

Support for this project was provided by the Alexander von Humboldt Foundation. We thank Lukas Becker for reading an early version of the manuscript and members of the Earth Surface Processes Modelling group at the GFZ for helpful feedback and discussions. Many figures were made using the R packages ggplot2 (Wickham, 2016), tmap (Tennekes, 2018), and rayshader (Morgan-Wall, 2020). All data included in the modelling has been previously published and is available in Amante & Eakins (2009), Baby et al. (2020), Belton & Raab (2010), Brown et al (1990 2002, 2014), Flowers & Schoene (2010), Green et al. (2017), Kounov et al. (2009, 2013), Raab et al. (2002), Stanley et al. (2013, 2015), Stanley & Flowers (2020) Tinker et al. (2008b), and Wildman et al. (2015, 2016, 2016). Data is summarized with publication information specified for individual data points in the supplemental materials. Code used to generate all model results is archived with Zenodo (Braun & Stanley, 2020) as is all of the input data, configuration, and results (Stanley, 2020).

References

Al-Hajri, Y., White, N., & Fishwick, S. (2009). Scales of transient convective support beneath Africa. *Geology*, *37*(10), 883–886. https://doi.org/10/fst5pn

Amante, C., & Eakins, B. W. (2009). ETOPO1 arc-minute global relief model: procedures, data sources and analysis.

Baby, G. (2017). Mouvements verticaux des marges passives d'Afrique australe depuis 130 Ma, étude couplée: stratigraphie de bassin: analyse des formes du relief.

Baby, G., Guillocheau, F., Morin, J., Ressouche, J., Robin, C., Broucke, O., & Dall'Asta, M. (2018). Post-rift stratigraphic evolution of the Atlantic margin of Namibia and South Africa: Implications for the vertical movements of the margin and the uplift history of the South African Plateau. *Marine and Petroleum Geology*, *97*, 169–191. https://doi.org/10/gfnc2j

Baby, G., Guillocheau, F., Boulogne, C., Robin, C., & Dall'Asta, M. (2018). Uplift history of a transform continental margin revealed by the stratigraphic record: The case of the Agulhas transform margin along the Southern African Plateau. *Tectonophysics*, *731–732*, 104–130. https://doi.org/10/gg6wn2

Baby, G., Guillocheau, F., Braun, J., Robin, C., & Dall'Asta, M. (2020). Solid sedimentation rates history of the Southern African continental margins: Implications for the uplift history of the South African Plateau. *Terra Nova*, *32*(1), 53–65. https://doi.org/10/ggw55p

Bamford, M. K., & Stevenson, I. R. (2002). A submerged Late Cretaceous podocarpaceous forest, west coast, South Africa : research letter. *South African Journal of Science*, *98*(3–4), 181–185.

Barnhart, K. R., Tucker, G. E., Doty, S., Shobe, C. M., Glade, R. C., Rossi, M. W., & Hill, M. C. (2020). Inverting topography for landscape evolution model process representation: Part 2, calibration and validation. *Journal of Geophysical Research: Earth Surface*, *n/a*(n/a), e2018JF004963. https://doi.org/10/ggnf59

Bell, D. R., Schmitz, M. D., & Janney, P. E. (2003). Mesozoic thermal evolution of the southern African mantle lithosphere. *Lithos*, *71*(2–4), 273–287. https://doi.org/10/chzs66

Belton, D. X., & Raab, M. J. (2010). Cretaceous reactivation and intensified erosion in the Archean–Proterozoic Limpopo Belt, demonstrated by apatite fission track thermochronology. *Tectonophysics*, *480*(1–4), 99–108. https://doi.org/10/fwqgqs

Bierman, P. R., Coppersmith, R., Hanson, K., Neveling, J., Portenga, E. W., & Rood, D. H. (2014). A cosmogenic view of erosion, relief generation, and the age of faulting in southern Africa. *GSA Today*, *24*(9), 4–11. https://doi.org/10/gg6w2n

Bluck, B. J., Ward, J. D., & De Wit, M. C. J. (2005). Diamond mega-placers: southern Africa and the Kaapvaal craton in a global context. *Geological Society, London, Special Publications*, *248*(1), 213–245. https://doi.org/10/bbmgfj

Braun, J. (2002). Quantifying the effect of recent relief changes on age–elevation relationships. *Earth and Planetary Science Letters*, *200*(3), 331–343. https://doi.org/10/fkcnn8

Braun, J. (2018). A review of numerical modeling studies of passive margin escarpments leading to a new analytical expression for the rate of escarpment migration velocity. *Gondwana Research*, *53*, 209–224. https://doi.org/10/gdb743

Braun, J., & Stanley, J. R. (2020). FastScape landscape evlolution model, fortran version utilized for southern African model inversions. Zenodo. http://doi.org/10.5281/zenodo.4150333

Braun, J., & Willett, S. D. (2013). A very efficient O (n), implicit and parallel method to solve the stream power equation governing fluvial incision and landscape evolution. *Geomorphology*, *180*, 170–179. https://doi.org/10/gbcbc9

Braun, J., Van Der Beek, P., & Batt, G. (2006). *Quantitative thermochronology: numerical methods for the interpretation of thermochronological data*. Cambridge University Press.

Braun, J., Robert, X., & Simon-Labric, T. (2013). Eroding dynamic topography. *Geophysical Research Letters*, *40*(8), 1494–1499. https://doi.org/10/gcpz7w

Braun, J., Guillocheau, F., Robin, C., Baby, G., & Jelsma, H. (2014). Rapid erosion of the Southern African Plateau as it climbs over a mantle superswell. *Journal of Geophysical Research: Solid Earth*, *119*(7), 6093–6112. https://doi.org/10/ggfrck

ten Brink, U., & Stern, T. (1992). Rift flank uplifts and Hinterland Basins: Comparison of the Transantarctic Mountains with the Great Escarpment of southern Africa. *Journal of Geophysical Research: Solid Earth*, *97*(B1), 569–585. https://doi.org/10/ckspp3

Brown, R. W., Rust, D. J., Summerfield, M. A., Gleadow, A. J., & De Wit, M. C. (1990). An Early Cretaceous phase of accelerated erosion on the south-western margin of Africa: Evidence from apatite fission track analysis and the offshore sedimentary record. *International Journal of Radiation Applications and Instrumentation. Part D. Nuclear Tracks and Radiation Measurements*, *17*(3), 339–350. https://doi.org/10/b7sq7r

Brown, R. W., Summerfield, M. A., & Gleadow, A. J. W. (2002). Denudational history along a transect across the Drakensberg Escarpment of southern Africa derived from apatite fission track thermochronology: DENUDATIONAL HISTORY OF THE

DRAKENSBERG ESCARPMENT. *Journal of Geophysical Research: Solid Earth*, *107*(B12), ETG 10-1-ETG 10-18. https://doi.org/10/dd579x

Brown, R. W., Summerfield, M., Gleadow, A., Gallagher, K., Carter, A., Beucher, R., & Wildman, M. (2014). Intracontinental deformation in southern Africa during the Late Cretaceous. *Journal of African Earth Sciences*, *100*, 20–41. https://doi.org/10/f6rd48

Burke, K. (1996). The african plate. *South African Journal of Geology*, *99*(4), 341–409.

Burke, K., & Gunnell, Y. (2008). *The African erosion surface: a continental-scale synthesis of geomorphology, tectonics, and environmental change over the past 180 million years* (Vol. 201). Geological Society of America.

Burke, K., & Wilson, J. T. (1972). Is the African Plate Stationary? *Nature*, *239*(5372), 387–389. https://doi.org/10/frb9xw

Catuneanu, O., Wopfner, H., Eriksson, P. G., Cairncross, B., Rubidge, B. S., Smith, R. M. H., & Hancox, P. J. (2005). The Karoo basins of south-central Africa. *Journal of African Earth Sciences*, *43*(1–3), 211–253. https://doi.org/10/br73kj

Chadwick, O. A., Roering, J. J., Heimsath, A. M., Levick, S. R., Asner, G. P., & Khomo, L. (2013). Shaping post-orogenic landscapes by climate and chemical weathering. *Geology*, *41*(11), 1171–1174. https://doi.org/10/gg6p2q

Chumakov, N. M., Zharkov, M. A., Herman, A. B., Doludenko, M. P., Kalandadze, N. N., Lebedev, E. L., et al. (1995). Climatic Belts of the Mid-Cretaceous Time. *Stratigraphy and Geological Correlation*, *3*(3), 42–63.

Cockburn, H. A. P., Seidl, M. A., & Summerfield, M. A. (1999). Quantifying denudation rates on inselbergs in the central Namib Desert using in situ–produced cosmogenic 10Be and 26Al. *Geology*, *27*(5), 399–402. https://doi.org/10/c9nmqx

Cockburn, H. A. P., Brown, R. W., Summerfield, M. A., & Seidl, M. A. (2000). Quantifying passive margin denudation and landscape development using a combined fission-track thermochronology and cosmogenic isotope analysis approach. *Earth and Planetary Science Letters*, *179*(3), 429–435. https://doi.org/10/dmssc4

Cohen, A. S., Coe, A. L., Harding, S. M., & Schwark, L. (2004). Osmium isotope evidence for the regulation of atmospheric CO2 by continental weathering. *Geology*, *32*(2), 157–160. https://doi.org/10/bcs23h

Colli, L., Stotz, I., Bunge, H.-P., Smethurst, M., Clark, S., Iaffaldano, G., et al. (2014). Rapid South Atlantic spreading changes and coeval vertical motion in surrounding continents: Evidence for temporal changes of pressure-driven upper mantle flow. *Tectonics*, *33*(7), 1304–1321. https://doi.org/10/ggtgh5

Conrad, C. P., & Molnar, P. (1997). The growth of Rayleigh—Taylor-type instabilities in the lithosphere for various rheological and density structures. *Geophysical Journal International*, *129*(1), 95–112. https://doi.org/10/cqzqbw

Cordonnier, G., Bovy, B., & Braun, J. (2019). A versatile, linear complexity algorithm for flow routing in topographies with depressions. *Earth Surface Dynamics*, *7*(2), 549–562. https://doi.org/10/ggk9xb

Cox, K. G. (1989). The role of mantle plumes in the development of continental drainage patterns. *Nature*, *342*(6252), 873–877. https://doi.org/10/fd34f6

Croissant, T., & Braun, J. (2014). Constraining the stream power law: a novel approach combining a landscape evolution model and an inversion method. *Earth Surface Dynamics*, *2*(1), 155–166. https://doi.org/10/gb9b78

Crowley, K. d, Cameron, M., & Schaefer, R. l. (1991). Experimental studies of annealing of etched fission tracks in fluorapatite. *Geochimica et Cosmochimica Acta*, *55*(5), 1449–1465. https://doi.org/10/ckh6js

Dauteuil, O., Bessin, P., & Guillocheau, F. (2015). Topographic growth around the Orange River valley, southern Africa: A Cenozoic record of crustal deformation and climatic change. *Geomorphology*, *233*, 5–19. https://doi.org/10/gg6w26

De Putter, T., & Ruffet, G. (2020). Supergene manganese ore records 75 Myr-long Campanian to Pleistocene geodynamic evolution and weathering history of the Central African Great Lakes Region–Tectonics drives, climate assists. *Gondwana Research*. https://doi.org/10/ghdn68

De Wit, M. C. J. (1988). Aspects of the geomorphology of the north-western Cape, South Africa. In *Geomorphological Studies in Southern Africa* (pp. 57–69). Rotterdam, Netherlands: CRC Press.

Decker, J. E., Niedermann, S., & de Wit, M. J. (2013). Climatically influenced denudation rates of the southern African plateau: Clues to solving a geomorphic paradox. *Geomorphology*, *190*, 48–60. https://doi.org/10/f4wwbs

Dessert, C., Dupré, B., Gaillardet, J., François, L. M., & Allègre, C. J. (2003). Basalt weathering laws and the impact of basalt weathering on the global carbon cycle. *Chemical Geology*, *202*(3–4), 257–273. https://doi.org/10/crx35j

Dietrich, P., & Hofmann, A. (2019). Ice-margin fluctuation sequences and grounding zone wedges: The record of the Late Palaeozoic Ice Age in the eastern Karoo Basin (Dwyka Group, South Africa). *The Depositional Record*, *5*(2), 247–271. https://doi.org/10/ghdn6x

Ding, X., Salles, T., Flament, N., Mallard, C., & Rey, P. F. (2019). Drainage and Sedimentary Responses to Dynamic Topography. *Geophysical Research Letters*, *46*(24), 14385–14394. https://doi.org/10/ggj9vp

Dingle, R., & Hendry, Q. (1984). Late Mesozoic and Tertiary sediment supply to the eastern Cape Basin (SE Atlantic) and palaeo-drainage systems in southwestern Africa. *Marine Geology*, *56*(1–4), 13–26. https://doi.org/10/c86r5c

Dingle, R. V., & Scrutton, R. A. (1974). Continental Breakup and the Development of Post-Paleozoic Sedimentary Basins around Southern Africa. *GSA Bulletin*, *85*(9), 1467–1474. https://doi.org/10/dw2dqs

Dirks, P. H. G. M., Placzek, C. J., Fink, D., Dosseto, A., & Roberts, E. (2016). Using 10Be cosmogenic isotopes to estimate erosion rates and landscape changes during the Plio-Pleistocene in the Cradle of Humankind, South Africa. *Journal of Human Evolution*, *96*, 19–34. https://doi.org/10/f8trm3

Dixey, F. (1955). Some aspects of the geomorphology of central and southern Africa. Geological Society of South Africa.

Doucouré, C. M., & de Wit, M. J. (2003). Old inherited origin for the present near-bimodal topography of Africa. *Journal of African Earth Sciences*, *36*(4), 371–388. https://doi.org/10/bxn5zr

Doucouré, C. M., Wit, M. J. de, & Mushayandebvu, M. F. (1996). Effective elastic thickness of the continental lithosphere in South Africa. *Journal of Geophysical Research: Solid Earth*, *101*(B5), 11291–11303. https://doi.org/10/d7t9q8

Duncan, R. A., Hooper, P. R., Rehacek, J., Marsh, J. S., & Duncan, A. R. (1997). The timing and duration of the Karoo igneous event, southern Gondwana. *Journal of Geophysical Research: Solid Earth*, *102*(B8), 18127–18138. https://doi.org/10/fgs8g6

Dupré, B., Dessert, C., Oliva, P., Goddéris, Y., Viers, J., François, L., et al. (2003). Rivers, chemical weathering and Earth's climate. *Comptes Rendus Geoscience*, *335*(16), 1141–1160. https://doi.org/10/c9sz48

Ebinger, C. J., & Sleep, N. H. (1998). Cenozoic magmatism throughout east Africa resulting from impact of a single plume. *Nature*, *395*(6704), 788–791. https://doi.org/10/cjqczh

Erlanger, E. D., Granger, D. E., & Gibbon, R. J. (2012). Rock uplift rates in South Africa from isochron burial dating of fluvial and marine terraces. *Geology*, *40*(11), 1019–1022. https://doi.org/10/gg6w2v

Farley, K. (2000). Helium diffusion from apatite: General behavior as illustrated by Durango fluorapatite. *Journal of Geophysical Research: Solid Earth*, *105*(B2), 2903–2914. https://doi.org/10/cgf34w

Flament, N., Gurnis, M., & Müller, R. D. (2013). A review of observations and models of dynamic topography. *Lithosphere*, *5*(2), 189–210. https://doi.org/10/f46573

Flament, N., Gurnis, M., Williams, S., Seton, M., Skogseid, J., Heine, C., & Dietmar Müller, R. (2014). Topographic asymmetry of the South Atlantic from global models of mantle flow and lithospheric stretching. *Earth and Planetary Science Letters*, *387*, 107–119. https://doi.org/10/gg3hzz

Fleming, A., Summerfield, M. A., Stone, J. O., Fifield, L. K., & Cresswell, R. G. (1999). Denudation rates for the southern Drakensberg escarpment, SE Africa, derived from in-situ-produced cosmogenic 36C1: initial results. *Journal of the Geological Society*, *156*(2), 209–212. https://doi.org/10/cmdjtb

Flowers, R. M., & Schoene, B. (2010). (U-Th)/He thermochronometry constraints on unroofing of the eastern Kaapvaal craton and significance for uplift of the southern African Plateau. *Geology*, *38*(9), 827–830. https://doi.org/10/bptpcp

Flowers, R. M., Ketcham, R. A., Shuster, D. L., & Farley, K. A. (2009). Apatite (U–Th)/He thermochronometry using a radiation damage accumulation and annealing model. *Geochimica et Cosmochimica Acta*, *73*(8), 2347–2365. https://doi.org/10/ffkmvz

Gallagher, K., & Brown, R. W. (1999a). Denudation and uplift at passive margins: the record on the Atlantic Margin of southern Africa. *Philosophical Transactions of the Royal Society of London. Series A: Mathematical, Physical and Engineering Sciences*, *357*(1753), 835–859. https://doi.org/10/ckc9sq

Gallagher, K., & Brown, R. W. (1999b). The Mesozoic denudation history of the Atlantic margins of southern Africa and southeast Brazil and the relationship to offshore sedimentation. *Geological Society, London, Special Publications*, *153*(1), 41–53. https://doi.org/10.1144/GSL.SP.1999.153.01.03

Garzanti, E., Dinis, P., Vermeesch, P., Andò, S., Hahn, A., Huvi, J., et al. (2018). Sedimentary processes controlling ultralong cells of littoral transport: Placer formation and termination of the Orange sand highway in southern Angola. *Sedimentology*, *65*(2), 431–460. https://doi.org/10/gcvdp9

Gilchrist, A. R., & Summerfield, M. A. (1990). Differential denudation and flexural isostasy in formation of rifted-margin upwarps. *Nature*, *346*(6286), 739–742. https://doi.org/10/bc9dsp

Gilchrist, A. R., Kooi, H., & Beaumont, C. (1994). Post-Gondwana geomorphic evolution of southwestern Africa: Implications for the controls on landscape development from observations and numerical experiments. *Journal of Geophysical Research: Solid Earth*, *99*(B6), 12211–12228. https://doi.org/10/cknczm

Glotzbach, C., Paape, A., Baade, J., Reinwarth, B., Rowntree, K., & Miller, J. (2016). Cenozoic landscape evolution of the Kruger National Park as derived from cosmogenic nuclide analyses. *Terra Nova*, *28*(5), 316–322. https://doi.org/10/f858tb

Göğüş, O. H., & Pysklywec, R. N. (2008a). Mantle lithosphere delamination driving plateau uplift and synconvergent extension in eastern Anatolia. *Geology*, *36*(9), 723–726. https://doi.org/10/c7pnrr

Göğüş, O. H., & Pysklywec, R. N. (2008b). Near-surface diagnostics of dripping or delaminating lithosphere. *Journal of Geophysical Research: Solid Earth*, *113*(B11). https://doi.org/10/bndzzs

Green, P. F., Duddy, I., Gleadow, A., Tingate, P., & Laslett, G. (1986). Thermal annealing of fission tracks in apatite: 1. A qualitative description. *Chemical Geology: Isotope Geoscience Section*, *59*, 237–253. https://doi.org/10/cjz3gv

Green, P. F., Duddy, I. R., Japsen, P., Bonow, J. M., & Malan, J. A. (2017). Post-breakup burial and exhumation of the southern margin of Africa. *Basin Research*, *29*(1), 96–127. https://doi.org/10/f9r64k

Guillocheau, F., Rouby, D., Robin, C., Helm, C., Rolland, N., Le Carlier de Veslud, C., & Braun, J. (2012). Quantification and causes of the terrigeneous sediment budget at the scale of a continental margin: a new method applied to the Namibia-South Africa margin: Quantification and causes of the terrigeneous sediment budget at the scale of a continental margin. *Basin Research*, *24*(1), 3–30. https://doi.org/10/bs34dc

Gurnis, M., Mitrovica, J. X., Ritsema, J., & Heijst, H.-J. van. (2000). Constraining mantle density structure using geological evidence of surface uplift rates: The case of the African Superplume. *Geochemistry, Geophysics, Geosystems*, *1*(7). https://doi.org/10/ck4zt8

Hansma, J., Tohver, E., Schrank, C., Jourdan, F., & Adams, D. (2016). The timing of the Cape Orogeny: New 40Ar/39Ar age constraints on deformation and cooling of the Cape Fold Belt, South Africa. *Gondwana Research*, *32*, 122–137. https://doi.org/10/f8n5n9

Hanson, E. K., Moore, J. M., Bordy, E. M., Marsh, J. S., Howarth, G., & Robey, J. V. A. (2009). CRETACEOUS EROSION IN CENTRAL SOUTH AFRICA: EVIDENCE FROM UPPER-CRUSTAL XENOLITHS IN KIMBERLITE DIATREMES. *South African Journal of Geology*, *112*(2), 125–140. https://doi.org/10/chqkp6

Hawthorne, J. (1975). Model of a kimberlite pipe. In *Physics and Chemistry of the Earth* (pp. 1–15). Elsevier.

Hay, W. W., & Floegel, S. (2012). New thoughts about the Cretaceous climate and oceans. *Earth-Science Reviews*, *115*(4), 262–272. https://doi.org/10/gdj3z7

Hoggard, M. J., White, N., & Al-Attar, D. (2016). Global dynamic topography observations reveal limited influence of large-scale mantle flow. *Nature Geoscience*, *9*(6), 456–463. https://doi.org/10/f8q6vq

Hopkins, A. E. (2006). Seismic stratigraphic interpretation of contourite systems.

Howard, A. D., & Kerby, G. (1983). Channel changes in badlands. *Geological Society of America Bulletin*, *94*(6), 739–752. https://doi.org/10/bd8c73

Howard, A. D., & Tierney, H. E. (2012). Taking the measure of a landscape: Comparing a simulated and natural landscape in the Virginia Coastal Plain. *Geomorphology*, *137*(1), 27–40. https://doi.org/10/cmmtj3

Hu, J., Liu, L., Faccenda, M., Zhou, Q., Fischer, K. M., Marshak, S., & Lundstrom, C. (2018). Modification of the Western Gondwana craton by plume–lithosphere interaction. *Nature Geoscience*, *11*(3), 203. https://doi.org/10/gc6nb9

Ibbitt, R. P., Willgoose, G. R., & Duncan, M. J. (1999). Channel network simulation models compared with data from the Ashley River, New Zealand. *Water Resources Research*, *35*(12), 3875–3890. https://doi.org/10/fhnscp

Jelsma, H. A., De Wit, M. J., Thiart, C., Dirks, P. H. G. M., Viola, G., Basson, I. J., & Anckar, E. (2004). Preferential distribution along transcontinental corridors of kimberlites and related rocks of Southern Africa. *South African Journal of Geology*, *107*(1–2), 301–324. https://doi.org/10/cdcnp5

Jenkyns, H. C., Forster, A., Schouten, S., & Sinninghe Damsté, J. S. (2004). High temperatures in the Late Cretaceous Arctic Ocean. *Nature*, *432*(7019), 888–892. https://doi.org/10/bwk64q

Johnson, M. R., Van Vuuren, C. J., Hegenberger, W. F., Key, R., & Show, U. (1996). Stratigraphy of the Karoo Supergroup in southern Africa: an overview. *Journal of African Earth Sciences*, *23*(1), 3–15. https://doi.org/10/bkhkqj

Jourdan, F., Féraud, G., Bertrand, H., Watkeys, M., & Renne, and P. (2008). The 40Ar/39Ar ages of the sill complex of the Karoo large igneous province: Implications for the Pliensbachian-Toarcian climate change. *Geochemistry, Geophysics, Geosystems*, *9*(6). https://doi.org/10/b4pwmp

Keen-Zebert, A., Tooth, S., & Stuart, F. M. (2016). Cosmogenic ^{3}He Measurements Provide Insight into Lithologic Controls on Bedrock Channel Incision: Examples from the South African Interior. *The Journal of Geology*, *124*(3), 423–434. https://doi.org/10/gg6w2w

King, L. C. (1942). South African scenery. A textbook of geomorphology. *South African Scenery. A Textbook of Geomorphology.*

King, L. C. (1950). The study of the world’s plainlands: a new approach in geomorphology. *Quarterly Journal of the Geological Society*, *106*(1–4), 101–131.

Kirby, E., & Whipple, K. X. (2012). Expression of active tectonics in erosional landscapes. *Journal of Structural Geology*, *44*, 54–75. https://doi.org/10/f4gm5d

Kounov, A., Niedermann, S., de Wit, M. J., Viola, G., Andreoli, M., & Erzinger, J. (2007). Present denudation rates at selected sections of the South African escarpment and the elevated continental interior based on cosmogenic 3He and 21Ne. *South African Journal of Geology*, *110*(2–3), 235–248. https://doi.org/10/fcx8hr

Kounov, A., Viola, G., de Wit, M., & Andreoli, M. A. G. (2009). Denudation along the Atlantic passive margin: new insights from apatite fission-track analysis on the western coast of South Africa. *Geological Society, London, Special Publications*, *324*(1), 287–306. https://doi.org/10/fg5592

Kounov, A., Viola, G., Dunkl, I., & Frimmel, H. E. (2013). Southern African perspectives on the long-term morpho-tectonic evolution of cratonic interiors. *Tectonophysics*, *601*, 177–191. https://doi.org/10/f47kxd

Kounov, A., Niedermann, S., De Wit, M. J., Codilean, A. T., Viola, G., Andreoli, M., & Christl, M. (2015). COSMOGENIC 21Ne AND 10Be REVEAL A MORE THAN 2 Ma ALLUVIAL FAN FLANKING THE CAPE MOUNTAINS, SOUTH AFRICA. *South African Journal of Geology*, *118*(2), 129–144. https://doi.org/10/f7r2qq

Linol, B., & De Wit, M. J. (2016). *Origin and Evolution of the Cape Mountains and Karoo Basin*. Springer.

Lithgow-Bertelloni, C., & Silver, P. G. (1998). Dynamic topography, plate driving forces and the African superswell. *Nature*, *395*(6699), 269–272. https://doi.org/10/fd5pfn

Macdonald, D., Gomez-Perez, I., Franzese, J., Spalletti, L., Lawver, L., Gahagan, L., et al. (2003). Mesozoic break-up of SW Gondwana: implications for regional hydrocarbon potential of the southern South Atlantic. *Marine and Petroleum Geology*, *20*(3–4), 287–308. https://doi.org/10/dzpzhq

Makhubela, T. V., Kramers, J. D., Scherler, D., Wittmann, H., Dirks, P. H. G. M., & Winkler, S. R. (2019). Effects of long soil surface residence times on apparent cosmogenic nuclide denudation rates and burial ages in the Cradle of Humankind, South Africa. *Earth Surface Processes and Landforms*, *44*(15), 2968–2981. https://doi.org/10/gg5s2s

Margirier, A., Braun, J., Gautheron, C., Carcaillet, J., Schwartz, S., Pinna Jamme, R., & Stanley, J. (2019). Climate control on Early Cenozoic denudation of the Namibian margin as deduced from new thermochronological constraints. *Earth and Planetary Science Letters*, *527*, 115779. https://doi.org/10/gf7tqs

Marsh, J., Hooper, P., Rehacek, J., Duncan, R., & Duncan, A. (1997). Stratigraphy and age of Karoo basalts of Lesotho and implications for correlations within the Karoo igneous province. *Geophysical Monograph-American Geophysical Union*, *100*, 247–272.

Martin, A. K., Goodlad, S. W., Hartnady, C. J. H., & Plessis, A. du. (1982). Cretaceous palaeopositions of the Falkland Plateau relative to southern Africa using Mesozoic seafloor spreading anomalies. *Geophysical Journal International*, *71*(3), 567–579. https://doi.org/10/bdgqrx

McMillan, I. (1990). A foraminiferal biostratigraphy and chronostratigraphy for the Pliocene to Pleistocene Upper Algoa Group, eastern Cape, South Africa. *South African Journal of Geology*, *93*(4), 622–622.

Molnar, P., Houseman, G. A., & Conrad, C. P. (1998). Rayleigh—Taylor instability and convective thinning of mechanically thickened lithosphere: effects of non-linear viscosity decreasing exponentially with depth and of horizontal shortening of the layer. *Geophysical Journal International*, *133*(3), 568–584. https://doi.org/10/b33r7p

Moore, A., & Verwoerd, W. (1985). The olivine melilitite-“kimberlite”-carbonatite suite of Namaqualand and Bushmanland, South Africa. *Transactions of the Geological Society of South Africa*, *88*(2), 281–294.

Moore, A. E. (1999). A reappraisal of epeirogenic flexure axes in southern Africa. *South African Journal of Geology*, *102*(4), 14.

Moore, A. E., Blenkinsop, T., & Cotterill, F. (Woody). (2009). Southern African topography and erosion history: plumes or plate tectonics? *Terra Nova*, *21*(4), 310–315. https://doi.org/10/fpr3b7

Morgan-Wall, T. (2020). rayshader: Create Maps and Visualize Data in 2D and 3D (Version 0.15.1). Retrieved from https://CRAN.R-project.org/package=rayshader

Moucha, R., & Forte, A. M. (2011). Changes in African topography driven by mantle convection. *Nature Geoscience*, *4*(10), 707–712. https://doi.org/10/cdhdg3

Müller, R. D., Royer, J.-Y., & Lawver, L. A. (1993). Revised plate motions relative to the hotspots from combined Atlantic and Indian Ocean hotspot tracks. *Geology*, *21*(3), 275–278. https://doi.org/10/df6g42

Nakashole, A. N., Hodgson, D. M., Chapman, R. J., Morgan, D. J., & Jacob, R. J. (2018). Long-term controls on continental-scale bedrock river terrace deposition from integrated clast and heavy mineral assemblage analysis: An example from the lower Orange River, Namibia. *Sedimentary Geology*, *364*, 103–120. https://doi.org/10/gc4fmp

Nunn, J. A., & Aires, J. R. (1988). Gravity anomalies and flexure of the lithosphere at the Middle Amazon Basin, Brazil. *Journal of Geophysical Research: Solid Earth*, *93*(B1), 415–428. https://doi.org/10/b25pdm

Nyblade, A. A., & Robinson, S. W. (1994). The African Superswell. *Geophysical Research Letters*, *21*(9), 765–768. https://doi.org/10/fmdpkk

Nyblade, A. A., & Sleep, N. H. (2003). Long lasting epeirogenic uplift from mantle plumes and the origin of the Southern African Plateau. *Geochemistry, Geophysics, Geosystems*, *4*(12). https://doi.org/10/b6xqks

O'Neill, C., Müller, D., & Steinberger, B. (2005). On the uncertainties in hot spot reconstructions and the significance of moving hot spot reference frames. *Geochemistry, Geophysics, Geosystems*, *6*(4). https://doi.org/10/ckb7jh

Osei Tutu, A., Steinberger, B., Sobolev, S. V., Rogozhina, I., & Popov, A. A. (2018). Effects of upper mantle heterogeneities on the lithospheric stress field and dynamic topography. *Solid Earth*, *9*(3), 649–668. https://doi.org/10/gdmt7w

Partridge, T. C., & Maud, R. R. (1987). Geomorphic evolution of southern Africa since the Mesozoic. *South African Journal of Geology*, *90*(2), 179–208.

Partridge, T. C., Dollar, E. S. J., Moolman, J., & Dollar, L. H. (2010). The geomorphic provinces of South Africa, Lesotho and Swaziland: A physiographic subdivision for earth and environmental scientists. *Transactions of the Royal Society of South Africa*, *65*(1), 1–47. https://doi.org/10/b8vz9j

Paul, J. D., Roberts, G. G., & White, N. (2014). The African landscape through space and time. *Tectonics*, *33*(6), 898–935. https://doi.org/10/f6ct3s

Pérez-Gussinyé, M., Metois, M., Fernández, M., Vergés, J., Fullea, J., & Lowry, A. R. (2009). Effective elastic thickness of Africa and its relationship to other proxies for lithospheric structure and surface tectonics. *Earth and Planetary Science Letters*, *287*(1), 152–167. https://doi.org/10/ftfcqp

Phillips, D., & Harris, J. W. (2009). Diamond provenance studies from 40Ar/39Ar dating of clinopyroxene inclusions: An example from the west coast of Namibia. *Lithos*, *112*, 793–805. https://doi.org/10/bcrxhs

Phillips, D., Harris, J. W., de Wit, M. C. J., & Matchan, E. L. (2018). Provenance history of detrital diamond deposits, West Coast of Namaqualand, South Africa. *Mineralogy and Petrology*, *112*(S1), 259–273. https://doi.org/10/gg6wp7

Pickford, M., Eisenmann, V., & Senut, B. (1999). Timing of landscape development and calcrete genesis in northern Namaqualand, South Africa, 3.

Ponte, J.-P., Robin, C., Guillocheau, F., Popescu, S., Suc, J.-P., Dall'Asta, M., et al. (2019). The Zambezi delta (Mozambique channel, East Africa): High resolution dating combining bio- orbital and seismic stratigraphies to determine climate (palaeoprecipitation) and tectonic controls on a passive margin. *Marine and Petroleum Geology*, *105*, 293–312. https://doi.org/10/gg2pjb

Pysklywec, R. N., & Mitrovica, J. X. (1999). The Role of Subduction-Induced Subsidence in the Evolution of the Karoo Basin. *The Journal of Geology*, *107*(2), 155–164. https://doi.org/10/fjc5r7

Raab, M. J., Brown, R. W., Gallagher, K., Carter, A., & Weber, K. (2002). Late Cretaceous reactivation of major crustal shear zones in northern Namibia: constraints from apatite fission track analysis. *Tectonophysics*, *349*(1–4), 75–92. https://doi.org/10/cd5b3t

Raab, M. J., Brown, R. W., Gallagher, K., Weber, K., & Gleadow, A. J. W. (2005). Denudational and thermal history of the Early Cretaceous Brandberg and Okenyenya igneous complexes on Namibia's Atlantic passive margin: EXHUMATION OF NAMIBIA'S PASSIVE MARGIN. *Tectonics*, *24*(3), n/a-n/a. https://doi.org/10/c6sgsg

Rayner, R. J., Bamford, M. K., Brothers, D. J., Dippenaar-Schoeman, A. S., McKay, I. J., Oberprieler, R. G., & Waters, S. B. (1997). CRETACEOUS FOSSILS FROM THE ORAPA DIAMOND MINE. *Palaeont. Afr.*, *33*, 55–65.

Renne, P. R., Glen, J. M., Milner, S. C., & Duncan, A. R. (1996). Age of Etendeka flood volcanism and associated intrusions in southwestern Africa. *Geology*, *24*(7), 659–662. https://doi.org/10/c4h9kz

Richardson, J. C., Hodgson, D. M., Paton, D., Craven, B., Rawcliffe, A., & Lang, A. (2017). Where is my sink? Reconstruction of landscape development in southwestern Africa since the Late Jurassic. *Gondwana Research*, *45*, 43–64. https://doi.org/10/f9zhv6

Roberts, D. L., Sciscio, L., Herries, A. I., Scott, L., Bamford, M. K., Musekiwa, C., & Tsikos, H. (2013). Miocene fluvial systems and palynofloras at the southwestern tip of Africa:

Implications for regional and global fluctuations in climate and ecosystems. *Earth-Science Reviews*, *124*, 184–201. https://doi.org/10/f494kc

Roberts, E. M., Stevens, N. J., O'Connor, P. M., Dirks, P. H. G. M., Gottfried, M. D., Clyde, W. C., et al. (2012). Initiation of the western branch of the East African Rift coeval with the eastern branch. *Nature Geoscience*, *5*(4), 289–294. https://doi.org/10/mhn

Roberts, G. G., & White, N. (2010). Estimating uplift rate histories from river profiles using African examples. *Journal of Geophysical Research: Solid Earth*, *115*(B2). https://doi.org/10/b3wrqz

Rouby, D., Bonnet, S., Guillocheau, F., Gallagher, K., Robin, C., Biancotto, F., et al. (2009). Sediment supply to the Orange sedimentary system over the last 150My: An evaluation from sedimentation/denudation balance. *Marine and Petroleum Geology*, *26*(6), 782–794. https://doi.org/10/bm25dp

Rubey, M., Brune, S., Heine, C., Davies, D. R., Williams, S. E., & Müller, R. D. (2017). Global patterns in Earth's dynamic topography since the Jurassic: the role of subducted slabs. *Solid Earth*, *8*(5), 899–919. https://doi.org/10/gcdj76

Rudge, J. F., Roberts, G. G., White, N. J., & Richardson, C. N. (2015). Uplift histories of Africa and Australia from linear inverse modeling of drainage inventories: RUDGE ET AL. *Journal of Geophysical Research: Earth Surface*, *120*(5), 894–914. https://doi.org/10/gg6wn3

Said, A., Moder, C., Clark, S., & Ghorbal, B. (2015). Cretaceous–Cenozoic sedimentary budgets of the Southern Mozambique Basin: Implications for uplift history of the South African Plateau. *Journal of African Earth Sciences*, *109*, 1–10. https://doi.org/10/f7mvxb

Sambridge, M. (1999). Geophysical inversion with a neighbourhood algorithm—I. Searching a parameter space. *Geophysical Journal International*, *138*(2), 479–494. https://doi.org/10/b84mkr

Sandersen, A. (2007). *A palynological investigation of the offshore Cretaceous sequence on the south-west coast of South Africa* (PhD). University of the Witswatersrand, Johannesburg, South Africa.

Scharf, T. E., Codilean, A. T., Wit, M. de, Jansen, J. D., & Kubik, P. W. (2013). Strong rocks sustain ancient postorogenic topography in southern Africa. *Geology*, *41*(3), 331–334. https://doi.org/10/f23vp5

Scheiber-Enslin, S. E., Ebbing, J., & Webb, S. J. (2015). NEW DEPTH MAPS OF THE MAIN KAROO BASIN, USED TO EXPLORE THE CAPE ISOSTATIC ANOMALY, SOUTH AFRICA. *South African Journal of Geology*, *118*(3), 225–248. https://doi.org/10/f72b79

Schmitz, M. D., & Bowring, S. A. (2003). Constraints on the thermal evolution of continental lithosphere from U-Pb accessory mineral thermochronometry of lower crustal xenoliths, southern Africa. *Contributions to Mineralogy and Petrology*, *144*(5), 592–618. https://doi.org/10/dpp9sd

Scholtz, A. (1985). The palynology of the upper lacustrine sediments of the Arnot Pipe, Banke, Namaqualand. *Annals of the South African Museum*, *95*(1), 1–109.

Senut, B., Pickford, M., & Ségalen, L. (2009). Neogene desertification of Africa. *Comptes Rendus Geoscience*, *341*(8), 591–602. https://doi.org/10/c8zb7x

Shuster, D. L., Flowers, R. M., & Farley, K. A. (2006). The influence of natural radiation damage on helium diffusion kinetics in apatite. *Earth and Planetary Science Letters*, *249*(3), 148–161. https://doi.org/10/c6nkx5

Skinner, C. J., Coulthard, T. J., Schwanghart, W., Wiel, M. J. V. D., & Hancock, G. (2018). Global sensitivity analysis of parameter uncertainty in landscape evolution models. *Geoscientific Model Development*, *11*(12), 4873–4888. https://doi.org/10/ggxjsd

Smith, R. (1986). Sedimentation and palaeoenvironments of Late Cretaceous crater-lake deposits in Bushmanland, South Africa. *Sedimentology*, *33*(3), 369–386. https://doi.org/10/drj8v3

Stanley, J. R. (2020). Model inputs and results from FastScape landscape evolution model runs for southern Africa [Data set]. Zenodo. http://doi.org/10.5281/zenodo.4153803

Stanley, J. R., & Flowers, R. M. (2020). Mesozoic denudation history of the lower Orange River and eastward migration of erosion across the southern African Plateau. *Lithosphere*. https://doi.org/10/ggjt45

Stanley, J. R., Flowers, R. M., & Bell, D. R. (2013). Kimberlite (U-Th)/He dating links surface erosion with lithospheric heating, thinning, and metasomatism in the southern African Plateau. *Geology*, *41*(12), 1243–1246. https://doi.org/10/f5pbr9

Stanley, J. R., Flowers, R. M., & Bell, D. R. (2015). Erosion patterns and mantle sources of topographic change across the southern African Plateau derived from the shallow and deep records of kimberlites. *Geochemistry, Geophysics, Geosystems*, *16*(9), 3235–3256. https://doi.org/10/f7zgxb

Steinberger, B. (2016). Topography caused by mantle density variations: observation-based estimates and models derived from tomography and lithosphere thickness. *Geophysical Journal International*, *205*(1), 604–621. https://doi.org/10/gg3h64

Steinberger, B., & Torsvik, T. H. (2008). Absolute plate motions and true polar wander in the absence of hotspot tracks. *Nature*, *452*(7187), 620–623. https://doi.org/10/c4pvr4

Steinberger, B., Conrad, C. P., Osei Tutu, A., & Hoggard, M. J. (2019). On the amplitude of dynamic topography at spherical harmonic degree two. *Tectonophysics*, *760*, 221–228. https://doi.org/10/ggzvt9

Stevenson, I. R., & McMillan, I. K. (2004). Incised valley fill stratigraphy of the Upper Cretaceous succession, proximal Orange Basin, Atlantic margin of southern Africa. *Journal of the Geological Society*, *161*(2), 185–208. https://doi.org/10/dp5bzq

Summerfield, M. A. (1983). Silcrete as a palaeoclimatic indicator: evidence from southern Africa. *Palaeogeography, Palaeoclimatology, Palaeoecology*, *41*(1), 65–79. https://doi.org/10/fmn95k

Svensen, H., Corfu, F., Polteau, S., Hammer, Ø., & Planke, S. (2012). Rapid magma emplacement in the Karoo Large Igneous Province. *Earth and Planetary Science Letters*, *325–326*, 1–9. https://doi.org/10/gg6wvq

Tennekes, M. (2018). tmap: Thematic Maps in R. *Journal of Statistical Software*, *84*(6), 1–39. https://doi.org/10/gfdd6z

Thiéblemont, A., Hernandez-Molina, F. J., Ponte, J.-P., Robin, C., Guillocheau, F., Cazzola, C., & Raisson, F. (2020). Seismic stratigraphic framework and depositional history for Cretaceous and Cenozoic contourite depositional systems of the Mozambique Channel, SW Indian Ocean. *Marine Geology*, *425*, 106192. https://doi.org/10/ghdn67

Tinker, J., de Wit, M., & Brown, R. W. (2008a). Linking source and sink: Evaluating the balance between onshore erosion and offshore sediment accumulation since Gondwana break-up, South Africa. *Tectonophysics*, *455*(1–4), 94–103. https://doi.org/10/ctp34n

Tinker, J., de Wit, M., & Brown, R. W. (2008b). Mesozoic exhumation of the southern Cape, South Africa, quantified using apatite fission track thermochronology. *Tectonophysics*, *455*(1–4), 77–93. https://doi.org/10/dw26sb

Uenzelmann-Neben, G., Schlüter, P., & Weigelt, E. (2007). Cenozoic oceanic circulation within the South African gateway: indications from seismic stratigraphy. *South African Journal of Geology*, *110*(2–3), 275–294. https://doi.org/10/ctvbzj

Van Der Beek, P., Summerfield, M. A., Braun, J., Brown, R. W., & Fleming, A. (2002). Modeling postbreakup landscape development and denudational history across the southeast African (Drakensberg Escarpment) margin. *Journal of Geophysical Research: Solid Earth*, *107*(B12), ETG 11-1-ETG 11-18. https://doi.org/10/cx7qnx

Watkins, C. E., & Conrad, C. P. (2018). Constraints on dynamic topography from asymmetric subsidence of the mid-ocean ridges. *Earth and Planetary Science Letters*, *484*, 264–275. https://doi.org/10/gc25h7

Whipple, K. X. (2004). Bedrock Rivers and the Geomorphology of Active Orogens. *Annual Review of Earth and Planetary Sciences*, *32*(1), 151–185. https://doi.org/10/dwkzhq

Whipple, K. X., & Tucker, G. E. (1999). Dynamics of the stream-power river incision model: Implications for height limits of mountain ranges, landscape response timescales, and research needs. *Journal of Geophysical Research: Solid Earth*, *104*(B8), 17661–17674. https://doi.org/10/brj8r8

Wickham, H. (2016). *ggplot2: Elegant Graphics for Data Analysis*. New York: Springer-Verlag. Retrieved from https://ggplot2.tidyverse.org

Wildman, M., Brown, R. W., Watkins, R., Carter, A., Gleadow, A., & Summerfield, M. (2015). Post break-up tectonic inversion across the southwestern cape of South Africa: New insights from apatite and zircon fission track thermochronometry. *Tectonophysics*, *654*, 30–55. https://doi.org/10/f7knvj

Wildman, M., Brown, R. W., Beucher, R., Persano, C., Stuart, F., Gallagher, K., et al. (2016). The chronology and tectonic style of landscape evolution along the elevated Atlantic continental margin of South Africa resolved by joint apatite fission track and (U-Th-Sm)/He thermochronology: Evolution of SW African Passive Margin. *Tectonics*, *35*(3), 511–545. https://doi.org/10/bcvn

Wildman, M., Brown, R., Persano, C., Beucher, R., Stuart, F. M., Mackintosh, V., et al. (2017). Contrasting Mesozoic evolution across the boundary between on and off craton regions of the South African plateau inferred from apatite fission track and (U-Th-Sm)/He thermochronology: Mesozoic Evolution of Southern Africa. *Journal of Geophysical Research: Solid Earth*, *122*(2), 1517–1547. https://doi.org/10/f9t9zx

Williams, L. S. (2015). Sedimentology of the Lower Cretaceous reservoirs of the Sea Lion Field, North Falkland Basin. *Petroleum Geoscience*, *21*(2–3), 183–198. https://doi.org/10/gg6w4n

Winterbourne, J., Crosby, A., & White, N. (2009). Depth, age and dynamic topography of oceanic lithosphere beneath heavily sedimented Atlantic margins. *Earth and Planetary Science Letters*, *287*(1–2), 137–151. https://doi.org/10/bv97vs

de Wit, M. C. J. (1999). Post-Gondwana drainage and the development of diamond placers in western South Africa. *Economic Geology*, *94*(5), 721–740. https://doi.org/10/fsz8gz

de Wit, M. (2007). The Kalahari Epeirogeny and climate change: differentiating cause and effect from core to space. *South African Journal of Geology*, *110*(2–3), 367–392. https://doi.org/10/bqc7x2

Zhang, N., Zhong, S., & Flowers, R. M. (2012). Predicting and testing continental vertical motion histories since the Paleozoic. *Earth and Planetary Science Letters*, *317–318*, 426–435. https://doi.org/10/bhrqhr

Journal of Geophysical Research: Solid Earth

Supporting Information for

Constraining plateau uplift in southern Africa by combining thermochronology, sediment flux, topography, and landscape evolution modeling

Jessica R. Stanley[1], Jean Braun[2,3], Guillaume Baby[4], François Guillocheau[5], Cécile Robin[5], Rebecca M. Flowers[6], Roderick Brown[7], Mark Wildman[7], Romain Beucher[8]

[1] Department of Geological Sciences, University of Idaho, 875 Perimeter Dr MS3022, Moscow ID 83843, USA.

[2] Helmholtz Centre Potsdam, GFZ German Research Center for Geosciences, Telegrafenberg Building A27, 14473 Potsdam, Germany.

[3] Institut für Erd- und Umweltwissenschaften, Universität Potsdam, 14476 Potsdam, Germany.

[4] Université de Paris, Institut de Physique du Globe de Paris, CNRS, F-75005, Paris, France.

[5] Université de Rennes 1, CNRS, Géosciences Rennes - UMR 6118, 35000 Rennes, France.

[6] Department of Geological Sciences, University of Colorado Boulder, UCB399, Boulder CO 80309, USA.

[7] School of Geographical and Earth Sciences, University of Glasgow, Glasgow, Scotland.

[8] Research School of Earth Sciences, The Australian National University, Canberra ACT 2600, Australia.

Contents of this file

Additional Supporting Information (Files uploaded separately)

Captions for Tables S1 and S2.
Caption for Movie S1.

Introduction

The supporting information includes summaries of the previously published thermochronology and sediment flux data used in the inversion models (Tables S1 and S2), uploaded separately. This document includes Figure S1 and Table S3, which are results and parameters used for the second inversion model testing only precipitation variability (see main text for more details. Also uploaded separately is a movie showing the landscape model topography for the best fit scenarios.

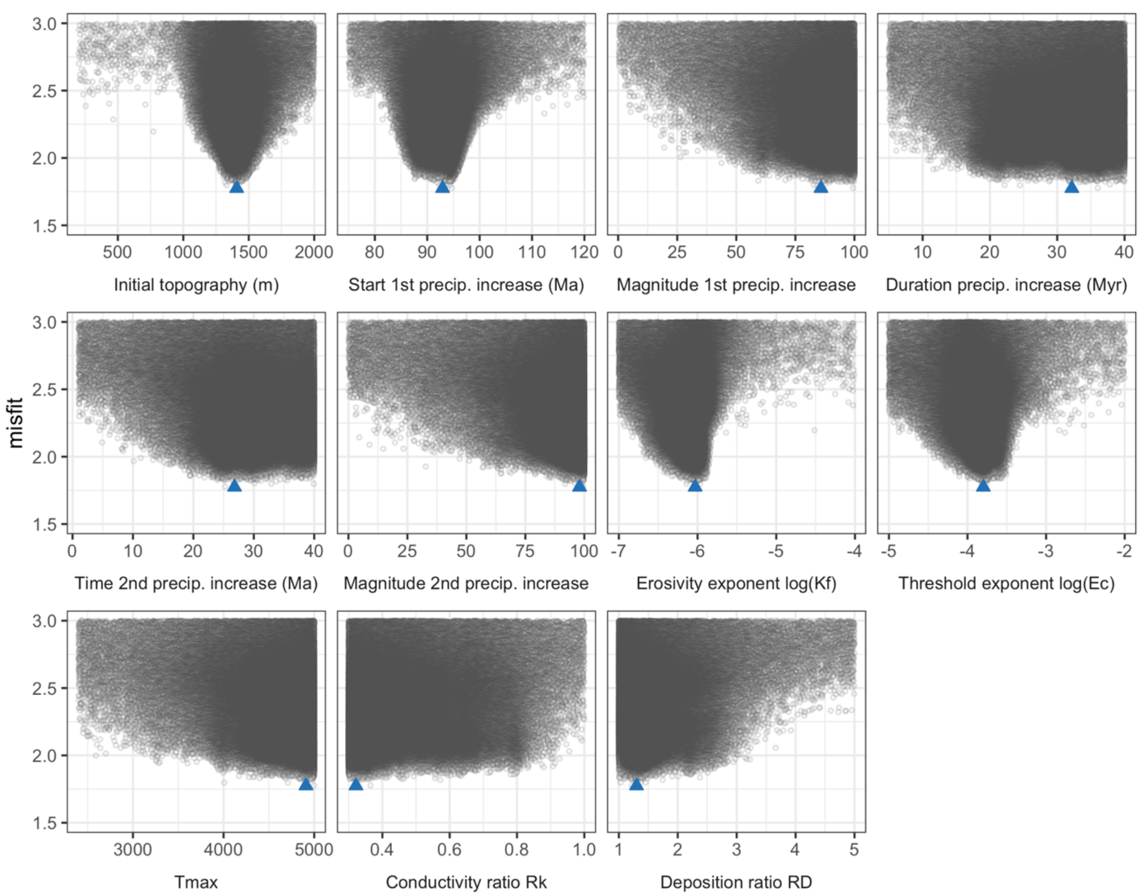

Figure S1. Results from model inversion testing only changes in precipitation (see Table S3 for parameter explanation). Plots show the values of parameters for models with misfits < 3. Each grey circle represents one forward model and the value for a given parameter. The lowest points show the parameters converging toward value(s) with better fits to the data. Blue triangles show best fit parameter values.

Table S1. Table S1. Thermochronology dates used in inversion model. AFT date and uncertainty represents the central age and 1σ standard deviation, while AHe date represents the average from multiple grains and uncertainty the 1σ standard deviation.

Table S2. Summary of the sediment flux data used in the model, originally published in Baby et al., (2020).

Variable Parameter	Units	Value Range	Precip best fit
K_f: Erosivity	$m^{0.2}$/yr	10^{-7} to 10^{-4}	9.325×10^{-7}
ε_c: Threshold for erosion	m/yr	10^{-5} to 10^{-2}	1.591×10^{-4}
T_{max}: Temperature at base of 120 km thick model lithosphere	°C	2400-5000	4909
R_k: Ratio of thermal conductivity between 2km thick Karoo sedimentary cover and underlying basement		0.3-1	0.322
R_D: Ratio between volume of material eroded and volume of material deposited in the marine basins		1-5	1.301
h_0: Height of initial base plateau in first time step	m	200-2000	1408
t_{p1}: Geologic time when first precipitation increase initiates	Ma	120-75	92.92
M_{p1}: Magnitude of first precipitation increase		0-100	83.83
t_{dur}: Duration of first precipitation increase before	Myr	5-40	32.17
t_{p2}: Geologic time of start of second precipitation increase	Ma	40-0	26.81
M_{p2}: Magnitude of second precipitation increase		0-100	97.98

Table S3. Variable parameters for precipitation driven inversion. Fixed parameters the same as in Table 2.

Movie S1. Movie showing topographic evolution from forward model runs for best fit model scenarios. Left panel shows results from the best fitting Hybrid Scenario, right panel shows best fitting result from the Cretaceous Scenario.